Modelling the steady-state motion of a soil column including nonlinear hysteretic damping under periodic excitations

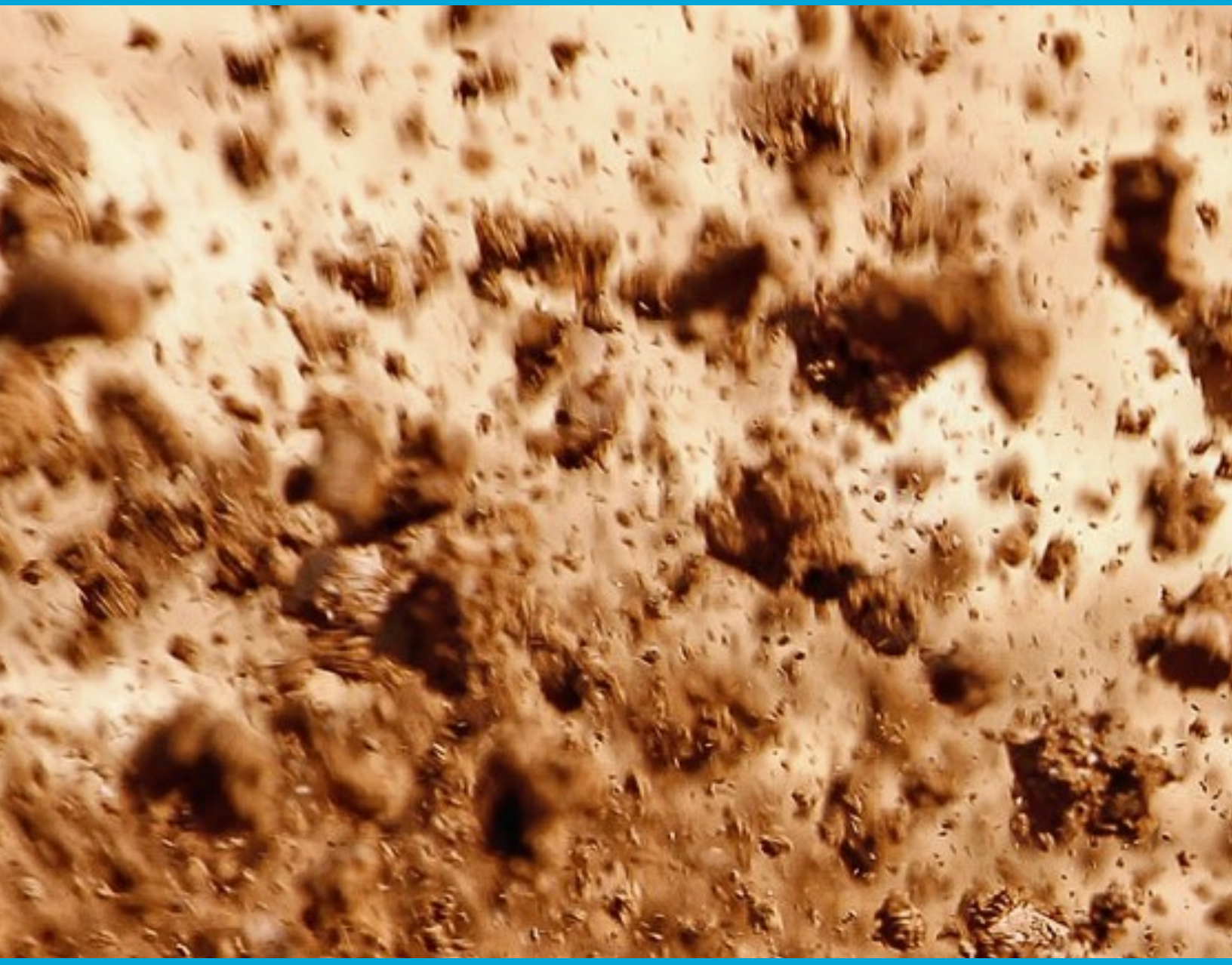

TU Delft

I.A. van der Esch

August 2020

Modelling the steady-state motion of a soil column including nonlinear hysteretic damping under periodic excitations

by

I.A. van der Esch

to obtain the degree of Master of Science
at the Delft University of Technology,
to be defended publicly on Wednesday August 26, 2020 at 15:00 PM.

Student number:	4497171	
Project duration:	August 19, 2019 – August 26, 2020	
Thesis committee:	Ir. A.B. Fărăgău	TU Delft, Daily supervisor
	Prof.dr. A.V. Metrikine	TU Delft, Supervisor
	Dr. F. Pisanò	TU Delft, Supervisor
	Dr.ir. K.N. van Dalen	TU Delft, Chairman

TU Delft
Faculty of Civil Engineering and Geosciences

This thesis is confidential and cannot be made public until August 26, 2025.

Abstract

Soil exhibits hysteretic damping. A commonly used implementation of this type of damping are the Masing rules. They consist of a loading and an unloading branch, defined as a piecewise function and having a nonsmooth character. This paper presents a framework how steady-state solutions of the motion of a soil column, with nonlinear hysteretic damping, can be obtained by using a variant of the Harmonic Balance Method (HBM), the Alternating Frequency/Time Harmonic Balance Method (AFTHBM), applied on a discretised soil column (a lattice system). The theoretical background of the method is presented, as well as its application to a soil column with both shear strain-dependent stiffness and damping. Results show that the AFTHBM is an efficient method for obtaining steady-state results for nonsmooth nonlinear behaviour, which is in this paper presented by simulations for nonlinear media. The results of the AFTHBM are sensitive to time sampling and convergence tolerances; nonetheless, if these parameters are properly chosen, the application of AFTHBM leads to good results.

Acknowledgements

By writing this part, I am finishing my research and want to take the opportunity to present my gratitude to all the people who support me in this thesis, in one way or another.

First of all, I want to thank my daily supervisor, Andrei Fărăgău, for all the support and useful insights. Without your help, the whole trajectory would be more difficult. Next, I want to present my gratitude to Karel van Dalen with his help, especially in the final stage of this research and giving me the possibility to present this thesis in the form of a paper. Also, I want to thank Andrei Metrikine and Federico Pisanò for their insightful comments during our meetings.

Next, I want to express my gratitude to Elise, for helping me relaxing after a busy day of checking the code for possible mistakes. Thank your parents too for their sincere interest, funny moments and serving me great meals during the corona-period.

Last but not least, my special thanks goes to my friends, family and especially my parents, which always supported me, no matter what. Thank you for your support throughout this adventure in Delft.

Anton van der Esch
Delft, August 2020

Contents

1 Introduction **1**
- 1.1 Nonlinear hysteretic damping & Masing rules 1
- 1.2 Computational methods for obtaining the response 2
- 1.3 Harmonic Balance Method 3
- 1.4 Alternating Frequency/Time Harmonic Balance Method . . . 4
- 1.5 Outline of this paper 5

2 Problem statement **5**
- 2.1 The description of the continuous soil column 5
- 2.2 Derivation of the hysteresis loops 6
- 2.3 Governing system of equations 7

3 Solution procedure **10**
- 3.1 Lumping procedure 10
- 3.2 AFTHBM procedure 10
- 3.3 Handling the transition points 15
- 3.4 Derivation of the transfer function for prescribed forces 16

4 Results **17**
- 4.1 Results based on the linear soil column 18
- 4.2 Results based on the nonlinear soil column 20

5 Conclusions and discussion **26**

Appendix A Derivation of the analytical derivatives of the hyperbolic soil model **29**
- Appendix A.1 Non-regularised nonlinear force definition 31
  - Appendix A.1.1 Terms of $\partial \mathbf{f}_{\mathrm{nl}}/\partial \mathbf{u}$ 31
  - Appendix A.1.2 Terms of $\partial \mathbf{u}/\partial \tilde{\mathbf{u}}$ 32
  - Appendix A.1.3 Terms of $\partial \mathbf{f}_{\mathrm{nl}}/\partial \dot{\mathbf{u}}$ 34
  - Appendix A.1.4 Terms of $\partial \dot{\mathbf{u}}/\partial \tilde{\mathbf{u}}$ 36
- Appendix A.2 Regularised nonlinear force definition 37
  - Appendix A.2.1 Terms of $\partial \mathbf{f}_{\mathrm{nl}}/\partial \mathbf{u}$ 37
  - Appendix A.2.2 Terms of $\partial \mathbf{u}/\partial \tilde{\mathbf{u}}$ 39
  - Appendix A.2.3 Terms of $\partial \mathbf{f}_{\mathrm{nl}}/\partial \dot{\mathbf{u}}$ 39
  - Appendix A.2.4 Terms of $\partial \dot{\mathbf{u}}/\partial \tilde{\mathbf{u}}$ 41

Appendix B Implementation of the Bouc-Wen model of hysteresis **42**
Appendix B.1 Introduction 42
Appendix B.2 Equations of motion 42
Appendix B.3 Case study 46

Appendix C Derivation of the analytical derivatives of the Bouc-Wen model **49**

1. Introduction

In this section, a small literature review is presented about the behaviour of the soil and the methods to calculate the response of the soil column.

1.1. Nonlinear hysteretic damping & Masing rules

Soil behaviour, which is often described by nonlinear constitutive models, contains strain dependent stiffness and damping. Under cyclic loading, the damping is hysteretic, so in case of strain-dependent damping, also the hysteretic damping becomes nonlinear. Hysteretic damping consists of a loading and an unloading branch, which shape depends on the backbone curve, governed by the applied material model [1]. The hysteretic damping exhibited by the soil, when the motion is in the steady-state, can be described by the Masing rules. They state that the hysteresis loops can be obtained by scaling the backbone curve with a factor two and move it to its reversal points, provided that the loadings are regular and with constant amplitude, which is the case in this paper [1, 2]. The Masing rules can be extended to non-steady responses, as done in the work of Jayakumar [3], but this is not in the scope of this paper. The Masing rules are widely applied in geomechanics and are, in this paper, based on the hyperbolic soil model, a relatively simple soil model, which is capable to describe nonlinear elastic behaviour proposed by Hardin and Drnevich [4, 5]. Other simple soil models, like the Davidenkov model, can exhibit unstable behaviour at very large strains [6], and are therefore not considered to prevent unnecessary convergence problems in the simulations. The backbone of the material model, which represents the relation between the shear strain and the shear stress, can only incorporate gradual stiffness changes, no stiffness jumps. However, when incorporating the Masing rules, the gradual changes dissappear at the transition points, these are points at where the loading branch turns into the unloading branch and vice versa. By applying the Masing rules on the hyperbolic soil model, the transition between those branches is nonsmooth due to C^0 continuity [7], which follows from the formulation of the nonlinear force (see Section 2). C^0 continuity requires special calculation procedures, as discussed in Subsection 1.4. In reality, the transition between the loading and the unloading branches is more smooth [8, 9], expecially for coarse-grained soils, because the shear stiffness related to the loading branch is not completely changed into the shear stiffness related to the unloading branch in an infinitesimal amount of time. Nonetheless, experiments show that the complete hysteresis loop

can be accurately descibed by the Masing rules, thus including C^0 continuity [2, 10].

1.2. Computational methods for obtaining the response

The motion of a nonlinear soil column is described by one nonlinear Partial Differential Equation (PDE) or a coupled system of nonlinear ODEs. To solve such systems of equations, multiple methods exist. Frequently applied methods are time-integration methods, such as the Newmark-Beta method, capable of solving both the transient state as well as the steady-state response. They are combined with a discretisation in space, which can be solved with a boundary value problem solver. For low damping, it takes relatively more time before the steady-state has been reached with respect to systems with a high amount of damping. Although time-integration methods can solve a large variety of problems, if one is interested only in the steady-state response, then the time-integration methods present drawbacks in perspective of the required computational time. Other common methods are equivalent linear methods [11], in which the nonlinear soil is approximated by a system of linear layers, thus yielding a system of linear PDEs. Each layer then contains a shear modulus and damping ratio which is independent of the shear strain. The applied value of the shear modulus and damping ratio are dependent on predefined reduction curves and are iterated until a certain accuracy has been reached. However, the nonlinear behaviour inside one soil layer is linearised which is not the case in reality. To circumvent the computation of the response in the time domain, approximation methods can be applied. Frequently applied methods for solving nonlinear problems are the method of multiple scales, the method of averaging and the Harmonic Balance Method (HBM) [12], in literature often referred to as the classical HBM [7]. The advantage of the HBM is that, in general, the steady-state solution can be obtained faster than with the other methods because the behaviour of the solution can be chosen a priori. In fact, HBM can be up to 10 times faster than conventional time-integration methods [13]. The principle of the HBM is that a truncated Fourier Series is substituted into the governing equations of motion. This leads to a system of nonlinear algebraic equations which can be solved for the unknown Fourier coefficients. Another advantage of HBM with respect to time-integration methods is that unstable solution branches of Frequency Response Curves (FRCs) in the steady-state can be detected, which is extremely difficult with time-integration methods. The Frequency Response Function (FRF) describes the relation between the amplitude of

motion and the forcing frequency. However, for nonlinear systems, multiple branches exist. They are sets of functions, and not a single function itself. Hence, for the Frequenc Response of nonlinear systems, is referred to the Frequency Response Curves (FRCs) [14, 15]. FRCs of nonlinear oscillators consist of multiple branches. This implies that the steady-state solutions of nonlinear systems are dependent on initial values which is not the case for purely linear systems. In some cases, the FRC can contain one or more unstable branches or even isolated branches [7, 16]. Like stated earlier, unstable branches are extremely difficult to detect with time-integration methods [17] but can be detected with the HBM in combination of path-continuation methods, like arc-length methods (methods of Riks, Chrisfield or Ritto-Correa Camotim [18, 19, 20, 21]) or amplitude-controlled algorithms which solves the system of nonlinear equations [17]. Besides unstable branches, even isolated branches can occur. A method to detect branching points, which are a type of a bifurcation point, is by making use of Floquet multipliers [7, 16], to characterise the bifurcation points. Although isolated branches can provide useful information about the state of the system, the treatment of those branches is not in the scope of this paper since they can occur in practice by slowly varying the excitation levels. This is not the type of excitation applied to the problem in this paper.

1.3. Harmonic Balance Method

In the previous paragraphs it has been stated why the HBM is an efficient tool to obtain the steady-state response for nonlinear vibration or wave propagation problems. The HBM is also often applied in the study of the behaviour of nonlinear oscillators. However, according to a paper, published in 1996 by Capecchi et al., which studied responses of hysteretic systems, the incorporation of hysteretic damping is much less addressed, especially in N-degree of freedom (NDOF) systems [22]. Some papers, which discuss the HBM incorporated with hysteretic damping in NDOF systems, are papers by Iwan [23]. These papers address hysteretic behaviour as both Masing rules as well as the Bouc-Wen model (for a method how this can be implemented is referred to Appendix B). For the last decades, more studies have been performed regarding single degree of freedom (SDOF) or NDOF hysteretic oscillators, especially from the contribution of Capecchi, Lacarbonara and Vestroni [24, 25, 26]. However, these papers do not deal with systems with more than two DOFs in combination of the HBM applied to Masing rules for the description applied to soil dynamics. Another and very recent paper

is that of Zhang et al. [27], which discusses the application of the HBM on finite and semi-infinite nonlinear dissipative continua which partly focuses on the study of the application of HBM to a continuous soil column. However, the damping model is not strain-dependent and the incorporated linear hysteretic damping is based on equivalent viscous damping [1], being related only to the dominant frequency which is not fully consistent. The current paper provides a framework on how nonlinear hysteretic damping can be incorporated in the HBM to obtain the response of soil with nonlinear elastic constitutive relations, based on the hyperbolic soil model which allows for a straightforward implementation [28]. Although the Masing rules overestimate the hysteretic damping at large strains ($\approx> 10^{-4} - 5 \cdot 10^{-4}$) [29, 2], or at high excitation frequencies at small strains ($< 10^{-5}$) [4], the Masing rules are adopted because they allow for a general description and thus implementation of the soil behaviour in the nonlinear elastic regime, which is the goal of this paper. Besides, those large shear strains are in the upper range or even above the cyclic treshold strain γ_t^c for which above the the assumption of soil being nonlinear elastic is no longer valid [4], implying that by applying the Masing rules the overestimation of the damping is limited.

1.4. Alternating Frequency/Time Harmonic Balance Method

In the classical HBM [7], which is a frequency-based method, the integrals which are needed to obtain the set of governing equations need to be in closed form. However, the magnitude of the internal nonlinear force, which results from the nonlinear constitutive model, is not of a polynomial type, which makes it cumbersome or even impossible to determine the transition times a prori, especially in the case of higher harmonics, so an iterative solution procedure is required. Moreover, because the nonlinear forces are nonsmooth, they cannot be directly evaluated in the frequency domain, so a conversion to the time domain is needed [30]. The Alternating Frequency/Time Harmonic Balance Method (AFTHBM) incorporates these features and is therefore applied in this paper. This method was first presented in 1989 by Cameron et al. [7]. The main difference of the AFTHBM with respect to the classical HBM is that the AFTHBM uses the Inverse Discrete Fourier Transform (IDFT) to evaluate the nonlinear force in the time domain and afterwards uses the Discrete Fourier Transform (DFT) to obtain the solution in the frequency domain, while the classical HBM directly evaluates the projections due to the closed form integrals. Furthermore, the AFTHBM is able to handle the unknown transition times, so it is not necessary to know

these transition times a priori by using event-driven schemes [7]. Employing these schemes can be a tedious task, because supplementary equations need to be provided [31], especially when higher order harmonics are taken into account since multiple loading and unloading phases can occur in a period [24]. Moreover, these schemes can only be applied for polynomial nonlinear and piecewise linear forces like dry-friction behaviour [7]. The AFTHBM is more suitable for application to these problems [32, 33], is superior in evaluating the nonlinear forces and obtaining its frequency components and has also proven its capacity for nonsmooth problems [34].

1.5. Outline of this paper

In this paper the AFTHBM is implemented in a soil column with nonlinear hysteretic behaviour. The applied constitutive model is the nonlinear elastic hyperbolic soil model. To allow a more straightforward implementation of this constitutive model, the soil column is discretised into a lattice system to obtain the governing equations of motions (EQMs). Displacements, hysteresis loops, spectra and FRCs are checked with a linear reference case and a Runge-Kutta method for time-integration with variable time steps [35].

2. Problem statement

In Section 1 a small literature study was provided. In this section the governing equations are derived, based on a 1D soil column on which the AFTHBM will be applied to obtain the steady-state response.

2.1. The description of the continuous soil column

The governing nonlinear PDE for a continuous soil column, with nonlinear constitutive behaviour (Figure 1), reads

$$\rho \frac{\partial^2 u\left(z,t\right)}{\partial t^2} = \frac{\partial}{\partial z}\left(\tau\left(z,t\right)\right), \tag{1}$$

with ρ the mass density in $\mathrm{kg}\cdot\mathrm{m}^{-3}$, z the depth, u the motion as a function of both z, all in m, $\gamma = \partial u/\partial u$ the shear strain, t the time in seconds and τ is the shear stress, expressed in $\mathrm{N}\cdot\mathrm{m}^{-2}$, and is given by

$$\tau\left(z,t\right) = G\left(\gamma\right)\gamma, \tag{2}$$

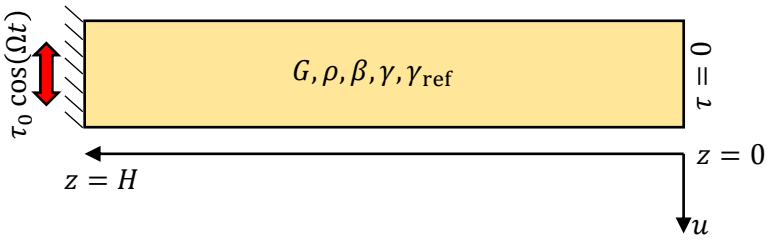

Figure 1: Continuous soil column. At the bottom $z = H$ the column is subjected to a prescribed stress $\tau = \tau_0 \cos(\Omega t)$ and at the top $z = 0$ the column is stress-free. The figure has been rotated 90 degrees clockwise.

where $G(\gamma)$ denotes the strain-dependent shear stiffness in $\mathrm{N} \cdot \mathrm{m}^{-2}$. Eq. (1) is subjected to a prescribed stress at the bottom $z = H$ and is stress free at the surface $z = 0$. Hence the boundary conditions read

$$\tau(z,t)\big|_{z=H} = \tau_0 \cos(\Omega t) \quad , \quad \tau(z,t)\big|_{z=0} = 0, \tag{3}$$

with H the height of the soil column, τ_0 the amplitude of the prescribed stress in $\mathrm{N} \cdot \mathrm{m}^{-2}$ and Ω the forcing frequency in radians per second (rad/s). $G(\gamma)$ is defined by a nonlinear constitutive law that describes the nonlinear elastic behaviour of the soil, according to

$$G(\gamma) = \frac{G_0}{1 + \left(\dfrac{|\gamma|}{\gamma_{\text{ref}}}\right)^{\beta}}, \tag{4}$$

where G_0 is the shear modulus at zero shear strain, β a curvature parameter [36, 37] and γ_{ref} the reference shear strain, often defined as the shear strain at $G(\gamma)/G_0 = 0.5$ [38], which influences the magnitude of the non-linearity [36]. The nonlinear elastic range for soil is approximately in the range of $\gamma = 10^{-5} - 10^{-4}$ which represents a $G(\gamma)/G_0 = 0.85$ at the cyclic treshold strain γ_{t}^{c} according to Eq. (4) [4].

2.2. Derivation of the hysteresis loops

The Masing rules are then obtained by scaling the backbone curve $f_{\text{bb}} = G(\gamma)\gamma$ with a factor two and shift it towards its reversal points [1], thus

$$\frac{\tau - \Delta\tau}{2} = f_{\text{bb}}\left(\frac{\gamma - \Delta\gamma}{2}\right), \tag{5}$$

where $\Delta\gamma$ and $\Delta\tau$ are the amplitudes of the cyclic shear strain and stress, respectively. The Masing rules can then be represented as

$$\tau = \begin{cases} \dfrac{G_0\left(\gamma + \Delta\gamma\right)}{1 + \left(\dfrac{|\gamma + \Delta\gamma|}{2\gamma_{\text{ref}}}\right)^{\beta}} - \Delta\tau & \text{if} \quad \dot{\gamma} > 0, \\ \dfrac{G_0\left(\gamma - \Delta\gamma\right)}{1 + \left(\dfrac{|\gamma - \Delta\gamma|}{2\gamma_{\text{ref}}}\right)^{\beta}} + \Delta\tau & \text{if} \quad \dot{\gamma} < 0, \end{cases} \tag{6}$$

where $\dot{\gamma}$ is the shear strain rate and the cyclic stress amplitude equals

$$\Delta\tau = \frac{G_0 \Delta\gamma}{1 + \left(\dfrac{|\Delta\gamma|}{\gamma_{\text{ref}}}\right)^{\beta}}. \tag{7}$$

The transition from the loading to the unloading branch is defined as the point where the sign of $\dot{\gamma}$ changes. Hence, Eq. (6) can be written in a more compact form like

$$\tau = \frac{G_0\left(\gamma + \operatorname{sgn}\left(\dot{\gamma}\right)\Delta\gamma\right)}{1 + \left(\dfrac{|\gamma + \operatorname{sgn}\left(\dot{\gamma}\right)\Delta\gamma|}{2\gamma_{\text{ref}}}\right)^{\beta}} - \frac{G_0 \operatorname{sgn}\left(\dot{\gamma}\right)\Delta\gamma}{1 + \left(\dfrac{\Delta\gamma}{\gamma_{\text{ref}}}\right)^{\beta}}. \tag{8}$$

Eq. (8) describes the nonlinear constitutive behaviour of the soil and exhibits C^0 continuity due to the appearance of the signum function. This implies there is a nonsmooth transition between the loading and the unloading branches. A typical hysteresis loop, described by Eq. (8), is depicted in Figure 2.

2.3. Governing system of equations

To obtain the response to the system, as described by Eqs. (1)-(4), the soil column is discretised into a NDOF system, see Figure 3. The governing equations of motion can then be readily obtained and are given by

$$\mathbf{M}\ddot{\mathbf{u}} + \mathbf{f}_{\text{nl}} = \mathbf{f}_{\text{ext}}, \tag{9}$$

with $\mathbf{M}$ the mass matrix and $\ddot{\mathbf{u}}$, $\mathbf{f}_{\text{ext}}$ and $\mathbf{f}_{\text{nl}}$ the acceleration, external force and nonlinear force vectors, respectively. Eq. (9) is discretised in space by

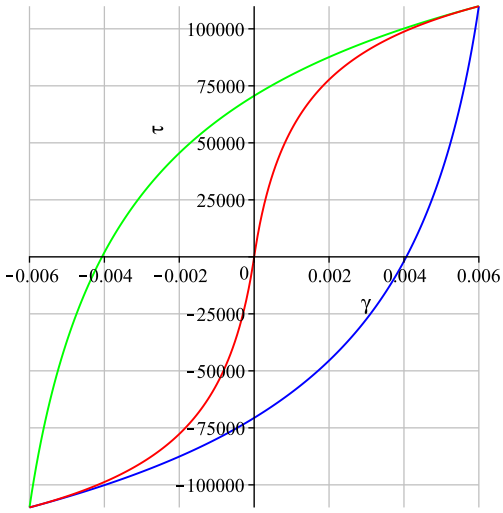

Figure 2: Hysteresis loop based on the hyperbolic soil model. —loading branch, $\dot{\gamma} > 0$. —unloading branch, $\dot{\gamma} < 0$. These branches are described by Eq. (6). —backbone curve, described by Eq. (4). Used parameters: $\gamma_{\text{ref}} = 1 \cdot 10^{-3}$, $\Delta\gamma = 6 \cdot 10^{-3}$, $\beta = 0.91$, $G_0 = 111.86 \cdot 10^6$ N $\cdot$ m^{-2}. The transition between the loading and unloading branch is nonsmooth (C^0 continuity).

lumping the continuous soil column. For the lumping procedure the reader is referred to Section 3. $\mathbf{M}$ is given by

$$\mathbf{M} = \begin{bmatrix} m_1 & 0 & \cdots & 0 \\ 0 & m_2 & & 0 \\ \vdots & \vdots & \ddots & \vdots \\ 0 & 0 & \cdots & m_N \end{bmatrix}, \tag{10}$$

and $\mathbf{f}_{\text{nl}}$ is obtained by using the displacement method. $f_{\text{nl}}^{(i)}$ contains a contribution from the internal forces $f_{\text{nl,int}}$ from the left side and right side of DOF (i), denoted as $^{(\alpha)}$ and $^{(\alpha+1)}$, respectively. Applying a positive displacement of DOF (i) will lead to a negative force contribution from the left and a positive force contribution from the right. Hence each component f_{nl}^{i} in $\mathbf{f}_{\text{nl}}$

can be described by

$$\begin{aligned} f_{\mathrm{nl}}^{(i)} &= f_{\mathrm{nl,int}}^{(\alpha)} - f_{\mathrm{nl,int}}^{(\alpha+1)}, \\ f_{\mathrm{nl,int}}^{(\alpha)} &= \frac{G_0 \left(\gamma^{(\alpha)} + \mathrm{sgn}\left(\dot{\gamma}^{(\alpha)}\right) \Delta\gamma^{(\alpha)}\right)}{1 + \left(\frac{|\gamma^{(\alpha)} + \mathrm{sgn}\left(\dot{\gamma}^{(\alpha)}\right) \Delta\gamma^{(\alpha)}|}{2\gamma_{\mathrm{ref}}}\right)^{\beta}} - \frac{G_0 \,\mathrm{sgn}\left(\dot{\gamma}^{(\alpha)}\right) \Delta\gamma^{(\alpha)}}{1 + \left(\frac{\Delta\gamma^{(\alpha)}}{\gamma_{\mathrm{ref}}}\right)^{\beta}}, \end{aligned} \tag{11}$$

with $\gamma^{(\alpha)}$ and $\dot{\gamma}^{(\alpha)}$ defined as the shear strain and shear strain rate at the internal point $\alpha = 1..N-1$ between DOFs $i = \alpha$ and $i = \alpha+1$, respectively. Therefore,

$$\gamma^{(\alpha)} = \frac{u^{(i+1)} - u^{(i)}}{\Delta z} \quad , \quad \dot{\gamma}^{(\alpha)} = \frac{\dot{u}^{(i+1)} - \dot{u}^{(i)}}{\Delta z} \quad , \quad \Delta\gamma^{(\alpha)} = \max_{p=0..M-1} \left(\gamma_p^{(\alpha)}\right), \tag{12}$$

with Δz the equidistant vertical spacing between the DOFs which is equal to

$$\Delta z = \frac{H}{N-1}. \tag{13}$$

To be able to apply the DFT and IDFT, the continuous time is discretised as well. $p = 1..M-1$ denotes the index of the considered time sample and M the number of applied time samples inside one period of oscillation. Assembling yields $\mathbf{f}_{\mathrm{nl}}$, given by

$$\mathbf{f}_{\mathrm{nl}} = \begin{bmatrix} -f_{\mathrm{nl,int}}^{(1)} \\ f_{\mathrm{nl,int}}^{(1)} - f_{\mathrm{nl,int}}^{(2)} \\ \vdots \\ f_{\mathrm{nl,int}}^{(N-2)} - f_{\mathrm{nl,int}}^{(N-1)} \\ f_{\mathrm{nl,int}}^{(N-1)} \end{bmatrix} = \begin{bmatrix} f_{\mathrm{nl}}^{(1)} \\ f_{\mathrm{nl}}^{(2)} \\ \vdots \\ f_{\mathrm{nl}}^{(N-1)} \\ f_{\mathrm{nl}}^{(N)} \end{bmatrix}. \tag{14}$$

$\mathbf{f}_{\mathrm{nl}}$ contains the complete constitutive behaviour, so no additional linear stiffness or damping has been provided like in the work of Wong et al. [17, 39]. The last vector in Eq. (9), $\mathbf{f}_{\mathrm{ext}}$, contains the components of the applied external forcing. For the soil column considered in this paper, all elements

inside $\mathbf{f}_{\text{ext}}$ are zero, except for DOF 1 which is subjected to a harmonic force according to Figure 3. Hence $\mathbf{f}_{\text{ext}}$ is given by

$$\mathbf{f}_{\text{ext}} = \left[f_{\text{ext}}^{(1)} \; 0 \; \cdots \; 0 \; 0 \right]^{\text{T}}. \tag{15}$$

3. Solution procedure

In Section 2 the governing equations of the problem were presented. In this section the solution procedure is highlighted. First the lumping procedure, which is required to obtain the governing set of equations, is explained, afterwards the approach of the AFTHBM is discussed in order to solve the governing equations. The section closes with the derivation of the transfer function for a soil column with prescribed forces to be able to interpret the results from the FRCs as presented in Section 4.

3.1. Lumping procedure

To obtain the correct mass at each DOF, a simple lumping model is applied, given by

$$m_i = \rho a_i. \tag{16}$$

This implies that the mass is lumped proportional to the associated height a_i of the element, where a_i is defined as the spacing between each element, given by

$$a_i = \begin{cases} \dfrac{H}{2\,(N-1)} & \text{if} \quad i = \{1, N\}\,, \\ \dfrac{H}{N-1} & \text{otherwise,} \end{cases} \tag{17}$$

with N the number of DOFs.

3.2. AFTHBM procedure

To determine the steady-state response of the soil column, which is assumed to be periodic, the AFTHBM is employed. As already mentioned, important to note is that the amplitude of the cyclic shear strain $\Delta\gamma^{(\alpha)}$ and the transition times from the loading to the unloading branch and vice versa are unknown a priori, see Eq. (8). To be able to solve this problem, an iterative procedure is required. In each iteration the nonlinear force vector

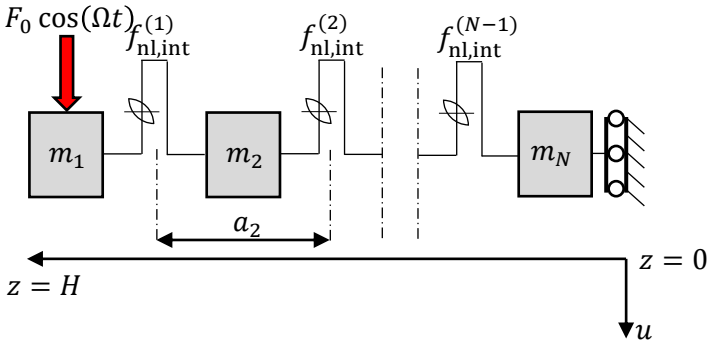

Figure 3: Lattice model of a soil column with hysteretic soil behaviour and prescribed forcing. The masses related to the DOFs are obtained by lumping. Note that the connection between each DOF only consist of a nonlinear element, so no additional linear stiffness or damping is provided. F_0 is the amplitude of the harmonic excitation, $F_{\text{nl,int}}^{(\alpha)}$ the nonlinear force between DOF (i) and $(i+1)$ with $i = \alpha+1$. a_i is the associated height to element (i). z indicates the depth and u the response. The figure has been rotated 90 degrees clockwise.

$\mathbf{f}_{\text{nl}}$, which contains $\Delta\gamma^{(\alpha)}$, is updated [40]. In this paper the procedure of Van Til et al. [34] has been followed and is summarized in Figure 4.

The procedure starts in the frequency domain, with the guess of an initial state vector $\tilde{\mathbf{u}}$

$$\tilde{\mathbf{u}} = [\mathbf{a}_0\ \mathbf{a}_1\ \mathbf{b}_1\ \cdots\ \cdots\ \mathbf{a}_j\ \mathbf{b}_j\ \cdots\ \cdots\ \mathbf{a}_J\ \mathbf{b}_J]^{\mathrm{T}}, \tag{18}$$

which describes the Fourier coefficients for the response at each DOF. In Eq. (18), $j = 1...J$ denotes the harmonic order, J the number of applied harmonics and

$$\begin{aligned}
\mathbf{a}_0 &= \left[a_0^{(1)}\ \cdots\ a_0^{(i)}\ \cdots\ a_0^{(N)}\right]^{\mathrm{T}}, \\
\mathbf{a}_j &= \left[a_j^{(1)}\ \cdots\ a_j^{(i)}\ \cdots\ a_j^{(N)}\right]^{\mathrm{T}}, \\
\mathbf{b}_j &= \left[b_j^{(1)}\ \cdots\ b_j^{(i)}\ \cdots\ b_j^{(N)}\right]^{\mathrm{T}},
\end{aligned} \tag{19}$$

are vectors which denote the Fourier coefficients associated to each degree of freedom $i = 1...N$ ($\mathbf{a}_0$, $\mathbf{a}_j$ and $\mathbf{b}_j$ are related to the constants, cosines and sines, respectively).

After assuming an initial state vector, they are transformed to the time

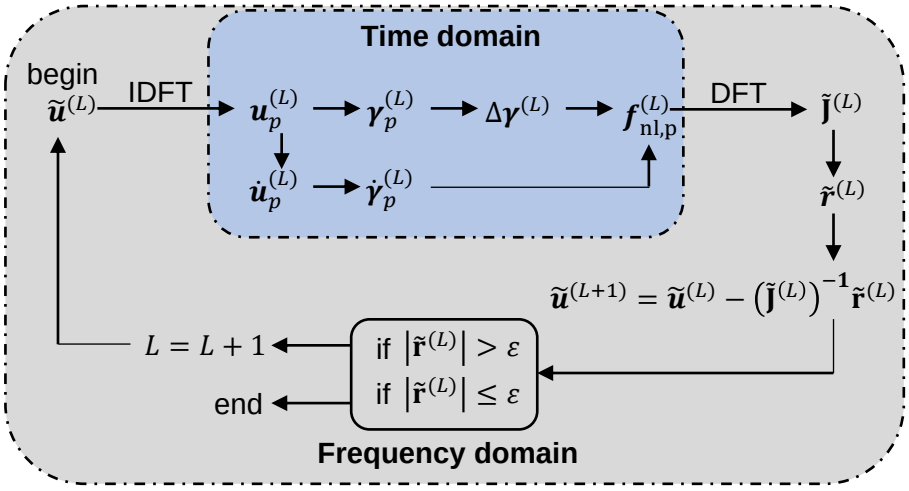

Figure 4: Principle of the AFTHBM. The procedure starts with assuming an initial ($L = 0$) state vector $\tilde{\mathbf{u}}$, see upper left, and ends when the tolerances are satisfied (bottom center). The scheme is borrowed and extended from the work of van Til [34] et al.

domain by the IDFT. The IDFT is given by

$$\mathbf{u}_p = \mathbf{a}_0 + \sum_{j=1}^{N_h} \left[\mathbf{a}_j \cos\left(j\Omega t_p\right) + \mathbf{b}_j \sin\left(j\Omega t_p\right)\right] \quad , \quad t_p = \frac{2\pi p}{M}. \tag{20}$$

Also, in the time domain, the nonlinear force (see Eq. (14)) is evaluated, which allows to handle the nonsmooth nonlinear force $\mathbf{f}_{\mathrm{nl}}$. Since $\mathbf{f}_{\mathrm{nl}}$ is also dependent on the velocities $\dot{\mathbf{u}}$, they need to be computed as well and can be readily obtained by forward, central and backward difference regarding the time samples p. Based on $\mathbf{u}$ and $\dot{\mathbf{u}}$, and by using Eq. (12), the shear strain vectors $\boldsymbol{\gamma}$, $\dot{\boldsymbol{\gamma}}$ and $\Delta\boldsymbol{\gamma}$ can be evaluated. The force is evaluated by substituting the obtained responses in the time domain according to Eq. (20) and substituting them into Eq. (14). The result is the nonlinear force evaluated in the time domain, denoted as $\mathbf{f}_{\mathrm{nl}}^{p}$. Also, in the time domain, the partial derivatives $\partial\mathbf{f}_{\mathrm{nl}}/\partial\tilde{\mathbf{u}}$ are computed. An overview of these derivatives are presented in Appendix A.

Next, the nonlinear force is transformed back to the frequency domain by using the DFT and denoted by its Fourier coefficients $\mathbf{c}_0$, $\mathbf{c}_j$ and $\mathbf{d}_j$ which denotes the 0-th harmonic, harmonics related to the cosines and sines, re-

spectively. They are given by

$$\mathbf{c}_0 = \frac{1}{M}\sum_{p=0}^{M-1}\mathbf{f}_{\mathrm{nl}}^{p}, \tag{21}$$

$$\mathbf{c}_j = \frac{2}{M}\sum_{p=0}^{M-1}\left[\mathbf{f}_{\mathrm{nl}}^{p}\cos\left(\frac{2\pi pj}{M}\right)\right],$$

$$\mathbf{d}_j = \frac{2}{M}\sum_{p=0}^{M-1}\left[\mathbf{f}_{\mathrm{nl}}^{p}\cos\left(\frac{2\pi pj}{M}\right)\right].$$

Simultaneously, the Jacobian $\tilde{\mathbf{J}}$ is computed in the frequency domain, requiring $\partial\mathbf{f}_{\mathrm{nl}}/\partial\tilde{\mathbf{u}}$. $\tilde{\mathbf{J}}$ is required to perform the iterative procedure to solve the system of nonlinear equations. This procedure is formed by using the Newton-Raphson method, given by

$$\tilde{\mathbf{u}}^{L+1} = \tilde{\mathbf{u}}^{L} - \left(\tilde{\mathbf{J}}^{L}\right)^{-1}\tilde{\mathbf{r}}^{L}, \tag{22}$$

where L denotes the number of the iteration, $\tilde{\mathbf{J}}^{L}$ the Jacobian and $\tilde{\mathbf{r}}$ the residual in the frequency domain, all evaluated at iteration L. The iterations are continued until

$$|\tilde{\boldsymbol{r}}| \leq \epsilon, \tag{23}$$

where ϵ is a tolerance, depending on J, M and N. Next, $\tilde{\mathbf{J}}$ is defined as

$$\tilde{\mathbf{J}} = \tilde{\mathbf{J}}_{\mathrm{L}} + \tilde{\mathbf{J}}_{\mathrm{nl}}, \tag{24}$$

where $\tilde{\mathbf{J}}_{\mathrm{L}}$ describes the inertial part of the Jacobian and $\tilde{\mathbf{J}}_{\mathrm{nl}}$ the Jacobian related to the nonlinear force of Eq. (9). They can be calculated as

$$\tilde{\mathbf{J}}_{\mathrm{L}} = \begin{bmatrix} \mathbf{0} & \mathbf{0} & \cdots & \mathbf{0} \\ \mathbf{0} & \tilde{\mathbf{J}}_{\mathrm{L}}^{(1)} & \cdots & \mathbf{0} \\ \vdots & \vdots & \ddots & \vdots \\ \mathbf{0} & \mathbf{0} & \cdots & \tilde{\mathbf{J}}_{\mathrm{L}}^{(J)} \end{bmatrix}, \quad \tilde{\mathbf{J}}_{\mathrm{L}}^{(j)} = \begin{bmatrix} -j^2\Omega^2\mathbf{M} & \mathbf{0} \\ \mathbf{0} & -j^2\Omega^2\mathbf{M} \end{bmatrix}, \tag{25}$$

$$\tilde{\mathbf{J}}_{\mathrm{nl}} = \left[\frac{\partial\mathbf{c}_0}{\partial\tilde{\mathbf{u}}}\ \frac{\partial\mathbf{c}_1}{\partial\tilde{\mathbf{u}}}\ \frac{\partial\mathbf{d}_1}{\partial\tilde{\mathbf{u}}}\ \cdots\ \cdots\ \frac{\partial\mathbf{c}_j}{\partial\tilde{\mathbf{u}}}\ \frac{\partial\mathbf{d}_j}{\partial\tilde{\mathbf{u}}}\ \cdots\ \cdots\ \frac{\partial\mathbf{c}_J}{\partial\tilde{\mathbf{u}}}\ \frac{\partial\mathbf{d}_J}{\partial\tilde{\mathbf{u}}}\right]^{\mathrm{T}},$$

where $\mathbf{c}$ and $\mathbf{d}$ were presented in Eq. (21). The elements of $\tilde{\mathbf{J}}_{\mathrm{nl}}$ can be calculated by using the DFT, hence

$$\begin{aligned}
\frac{\partial \mathbf{c}_0}{\partial \tilde{\mathbf{u}}} &= \frac{1}{M} \sum_{p=0}^{M-1} \frac{\partial \mathbf{f}_{\mathrm{nl}}}{\partial \tilde{\mathbf{u}}}, \\
\frac{\partial \mathbf{c}_j}{\partial \tilde{\mathbf{u}}} &= \frac{2}{M} \sum_{p=0}^{M-1} \left[\frac{\partial \mathbf{f}_{\mathrm{nl}}}{\partial \tilde{\mathbf{u}}} \cos\left(\frac{2\pi p j}{M}\right) \right], \\
\frac{\partial \mathbf{d}_j}{\partial \tilde{\mathbf{u}}} &= \frac{2}{M} \sum_{p=0}^{M-1} \left[\frac{\partial \mathbf{f}_{\mathrm{nl}}}{\partial \tilde{\mathbf{u}}} \sin\left(\frac{2\pi p j}{M}\right) \right].
\end{aligned} \tag{26}$$

The partial derivatives of the nonlinear force with respect to its state vector, $\partial \mathbf{f}_{\mathrm{nl}} / \partial \tilde{\mathbf{u}}$ in Eq. (26), are computed by means of the chain rule

$$\frac{\partial \mathbf{f}_{\mathrm{nl}}\left(\mathbf{u}, \dot{\mathbf{u}}\right)}{\partial \tilde{\mathbf{u}}} = \frac{\partial \mathbf{f}_{\mathrm{nl}}}{\partial \mathbf{u}} \, \frac{\partial \mathbf{u}}{\partial \tilde{\mathbf{u}}} + \frac{\partial \mathbf{f}_{\mathrm{nl}}}{\partial \dot{\mathbf{u}}} \, \frac{\partial \dot{\mathbf{u}}}{\partial \tilde{\mathbf{u}}}. \tag{27}$$

Eq. (27) contains partial derivatives with respect to both $\mathbf{u}$ and $\dot{\mathbf{u}}$ since the state vector depends on these quantities. Important to note is that these derivatives are evaluated in the time domain and derived analytically using MAPLE and are presented in Appendix A. Computing them analytically instead of numerically lowers the computational costs [33]. Besides, computation of the derivatives numerically would reduce accuracy, especially in regions where the nonlinear force is nonsmooth.

The last step inside one iteration is the formulation of the residual functions to be able to solve the system iteratively. They consist of $N\left(2J+1\right)$ equations and are formulated by balancing the Fourier coefficients for both constants, cosines and sines, respectively, and are given by

$$\begin{aligned}
\tilde{\mathbf{r}}_0 &= \mathbf{c}_0 - \mathbf{f}_{\mathrm{ext}}^0 = \mathbf{0}, \\
\tilde{\mathbf{r}}_j^{\cos} &= -j^2 \Omega^2 \mathbf{M} \mathbf{a}_j + \mathbf{c}_j - \mathbf{f}_{\mathrm{ext}}^{\cos} = \mathbf{0}, \\
\tilde{\mathbf{r}}_j^{\sin} &= -j^2 \Omega^2 \mathbf{M} \mathbf{b}_j + \mathbf{d}_j - \mathbf{f}_{\mathrm{ext}}^{\sin} = \mathbf{0}.
\end{aligned} \tag{28}$$

Now the steady-state motion of the system is fully determined. An overview of the procedure is presented in Figure 4.

3.3. Handling the transition points

Due to the nonsmooth transition from the loading to the unloading branch, signum functions occur in $\mathbf{f}_{\mathrm{nl}}$, see Eq. (8). By taking partial derivatives of these signum functions, Dirac delta functions $\delta(u)$ appear since

$$\frac{\partial}{\partial t}\operatorname{sgn}(u) = 2\delta(u). \tag{29}$$

Due to sampling, a sampling point p is exactly evaluated at this transition point, leading to singularities in the implementation, which is not physical. For resolving this problem, multiple solutions exist.

Krack et al. [41] showed a method to make use of a high-order harmonic balance method in combination with direct calculation of the transition time moments for prevention of singularities or using a mixed-shooting HBM. However, this is not implemented in this paper since the goal is to formulate a straightforward implementation and give the reader insight in this method. Another and more straightforward method is to recognize that when the partial derivatives are derived according to Eq. (A.2), the DFT is applied to obtain $\tilde{\mathbf{J}}$, see Eq. (26). By putting an additional condition that the partial derivatives are zero at the reversal points, the singularity is circumvented. However, this is not exactly the case and leads to some errors. A way to overcome this is to recognize that the DFT is a discretised version of the Fourier Transform (FT), so one could make use of the Sifting property [42] to evaluate the FT at the reversal points.

It is also possible to use regularisation or smoothing in the formulation of the nonlinear force [7]. Joannin et al. makes use of this principle by using a regularization parameter ε, applied on a system with Coulomb dry friction, leading to a more smooth description of the nonlinear force [33, 43]. By applying regularisation the signum function is approximated with a tanh function which yields the signum function only in the limit case

$$\lim_{\varepsilon \longrightarrow 0}\left[\tanh\left(\frac{u}{\epsilon}\right)\right] = \operatorname{sgn}(u). \tag{30}$$

Applying Eq. (30) to Eq. (11) yields

$$f_{\mathrm{nl}}^{(i)} = f_{\mathrm{nl,int}}^{(\alpha)} - f_{\mathrm{nl,int}}^{(\alpha+1)}, \tag{31}$$

$$f_{\mathrm{nl,int}}^{(\alpha)} = \frac{G_0\left(\gamma^{(\alpha)} + \tanh\left(\dot{\gamma}^{(\alpha)}/\varepsilon\right)\Delta\gamma^{(\alpha)}\right)}{1+\left(\frac{\left|\gamma^{(\alpha)} + \tanh\left(\dot{\gamma}^{(\alpha)}/\varepsilon\right)\Delta\gamma^{(\alpha)}\right|}{2\gamma_{\mathrm{ref}}}\right)^{\beta}} - \frac{G_0\tanh\left(\dot{\gamma}^{(\alpha)}/\varepsilon\right)\Delta\gamma^{(\alpha)}}{1+\left(\frac{\Delta\gamma^{(\alpha)}}{\gamma_{\mathrm{ref}}}\right)^{\beta}}.$$

The advantage of regularisation is that it directly can be implemented without any additional computational effort and therefore this method is applied in this paper. However, the choice of ε is not arbitrary, choosing it too large will drift the solution away from the results as obtained with signum functions. On the other hand, a small ε will cease the smoothing effect because the signum function is better approximated.

3.4. Derivation of the transfer function for prescribed forces

To get more insight in the behaviour of the system, and to be able to compare the nonlinear system with the linear reference case, the transfer function for the linear soil column with prescribed forces is derived. Applying the Fourier Transform (FT) on the linear version of Eq. (1), and solving for the magnitude of the motion in the frequency domain, $U(z,\omega)$, yields

$$U(z,\omega) = Ae^{-ik_{\mathrm{s}}z} + Be^{ik_{\mathrm{s}}z}, \tag{32}$$

where $k_{\mathrm{s}} = \omega/c_{\mathrm{s}}$ denotes the wave number in rad/m, ω the radial frequency in rad/s, $c_s = \sqrt{G_0/\rho}$ the propagation speed of the shear waves in m/s and $i = \sqrt{-1}$ the imaginary unit. Applying the boundary conditions (see Eq. (3)) on Eq. (32) yields

$$U(z,\omega) = \frac{\cos(k_{\mathrm{s}}z)}{\sin(k_{\mathrm{s}}H)}F_{\mathrm{b}}(\omega). \tag{33}$$

with F_{b} the prescribed force of the soil column at the base, which equals τ in Eq. (3) in case of a unit square area $A = 1\ \mathrm{m}^2$. The transfer function

$$\frac{\cos(k_{\mathrm{s}}z)}{\sin(k_{\mathrm{s}}H)} \tag{34}$$

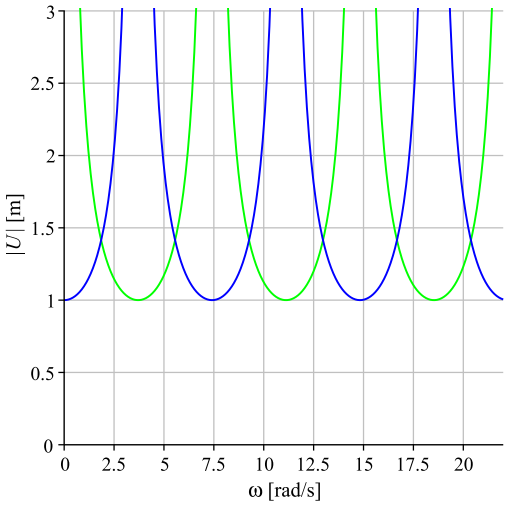

Figure 5: Transfer functions plotted at the free surface, $z = 0$. —Transfer function in case of prescribed forces. —Transfer function in case of prescribed displacements. Note that for $\omega = 0$ an infinite displacement is imposed in case of prescribed forces. Used parameters in this analysis: $H = 100$ m, $G_0 = 111.86 \cdot 10^6$ N $\cdot$ m^{-2}, $\rho = 2009.8$ kg $\cdot$ m $^{-2}$, $z = 0$ m.

is plotted at the free surface, and compared with the transfer function for a prescribed displacement in Figure 5. Resonance occurs if the denominator equals 0, hence the eigenfrequencies of the $n-$th mode can be calculated according to

$$\omega_n = n\pi \frac{\sqrt{G_0/\rho}}{H}. \tag{35}$$

This property is used in Subsections 4.1 and 4.2, where the analysis are performed close to the first eigenfrequency ($n = 1$) of the linear system. According to the parameters of the analysis, see the caption of Figure 6 and Eq. (35), the first two eigenfrequencies $n = 1, 2$ are

$$\omega_1 = 7.41 \text{ rad/s} \quad , \quad \omega_2 = 14.82 \text{ rad/s}. \tag{36}$$

4. Results

In this section the results of the simulations are presented, based both on a soil column with linear constitutive behaviour and nonlinear constitu-

tive behaviour, i.e. nonlinear hysteretic damping, subjected to a prescribed force. Both cases are checked by a time-integration method (ODE45 from MATLAB).

4.1. Results based on the linear soil column

For validation purposes, first a soil column is analysed but based on linear behaviour, subjected to harmonic excitation close to the first eigenfrequency ($\Omega = 8$ rad/s vs. $\omega_1 = 7.41$ rad/s), but not exactly at the first eigenfrequency, to guarantee convergence. This makes the validation process more robust since discrepancies in the model becomes more apparent due to the magnifying character of the response in this region. Regarding a soil column with linear elastic behaviour, the hyperbolic soil model exhibits linear behaviour when

$$\lim_{\gamma_{\text{ref}} \longrightarrow \infty} \left[\frac{G_0}{1 + \left(\dfrac{|\gamma|}{\gamma_{\text{ref}}} \right)^{\beta}} \right] = G_0, \tag{37}$$

so a $\gamma_{\text{ref}} = 100$ has been applied. The validity of this number has been checked by considering a normalised secant shear stiffness $\overline{G}_{\text{sec}}$, defined as

$$\overline{G}_{\text{sec}} = \frac{G_{\text{sec}}}{G_0} \quad , \quad G_{\text{sec}} = \frac{\Delta\tau}{\Delta\gamma}. \tag{38}$$

For the linear limit case, $\overline{G}_{\text{sec}}$ is presented in Figure 6. Its value over the whole height of the soil column is close to 1, proving the validity of the chosen γ_{ref}. The motion u of the converged linear column (for which the same parameters are applied as in Figure 6) are compared with the linear soil model where $G = G_0$. The results coincide, confirming the validity of the model in the linear limit case. Moreover, the motion has been additionally checked with a time-integration method, ODE45 in MATLAB, which also coincides with the results as obtained by the AFTHBM. The results for the motions are plotted for DOF 30, because in a later stage it will appear that in the neighbourhood of this DOF the highest shear strain (thus nonlinearity) in the soil column occur, demonstrating the capability of the model to deal with large nonlinearities.

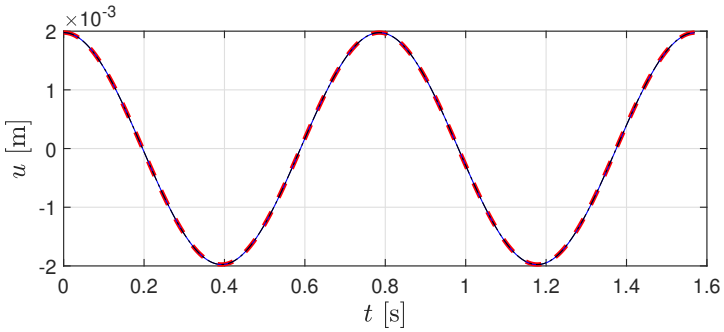

(a) Displacements in the soil column at DOF 30, $z = 40.82$ m, $z_{\mathrm{b}} = 59.18$ m.

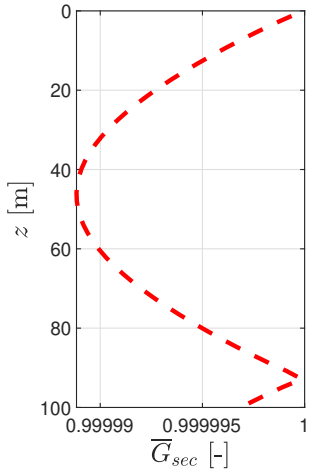

(b) $\overline{G}_{\mathrm{sec}}$.

Figure 6: Analysis of the linear limit case. (a) Motion at DOF 30. (b) Stiffness reduction along the soil column, expressed in terms of $\overline{G}_{\mathrm{sec}}$. - - -Motion computed by AFTHBM. -·-·-motion of the linear system. ——Time-integration results by using ODE45 in MATLAB. Used parameters in this simulation: $H = 100$ m, $N = 50$, $\Omega = 8$ rad/s, $J = 1$, $\gamma_{\mathrm{ref}} = 100$, $\beta = 0.91$, $G_0 = 111.86 \cdot 10^6$ N $\cdot$ m^{-2}, $\rho = 2,009.8$ kg $\cdot$m^{-3}, $M = 2^9$, $F_0 = 10,000$ N, $\epsilon = 10^{-9}$.

4.2. Results based on the nonlinear soil column

Besides considering the linear limit case, the soil column has also been checked with the aforementioned time-integration method. For this simulation the same parameters as for the linear limit case have been used, except for $\gamma_{\text{ref}} = 8.7 \cdot 10^{-4}$, see Figure 7. With time-integration methods, both the transient as well as the steady-state regime of the response are computed. Considering $\mathbf{f}_{\text{nl}}$, as derived in Eq. (11), implies that the nonlinear force is dependent on $\Delta\gamma$, which is obtained from a previous simulation. Hence, to obtain the steady-state solution by applying time-integration, multiple simulations need to be performed, where $\Delta\gamma$ forms the input of the next simulation, provided that the steady-state has been reached. In other words, the steady-state solution needs to be sought in an iterative way with the time-integration method. This is a very computational demanding procedure or even impossible. To still be able to get results for a time-integration method with relatively small computational times, the vectors $\mathbf{u}$ and $\dot{\mathbf{u}}$ from the AFTHBM simulations are used as initial conditions for the time-integration to suppress the transient phase. Approximating these initial conditions as best as possible, the initial conditions with respect to the time derivatives of u are obtained with central difference of the AFTHBM results. Even then, there are some differences in the amplitude of motion since the time-stepping from ODE45 is considerably smaller, leading to possible evaluations of the nonlinear force at the other branch than AFTHBM. Moreover, the nonlinear force definition of the time-integration contains still the $\Delta\gamma$ values obtained in the AFTHBM method. Combined, this can drift the solution based on the time-integration away when the steady-state is not perfectly reached from $t = 0$ s, hence the time-integration results are very sensitive to the applied initial conditions.

The results computed by the AFTHBM at DOF 30, as well as with the time-integration and the linear limit case, are presented in Figure 7a. The amplitude of the motion of the nonlinear case is much smaller compared to the linear system, which is reasonable since hysteretic damping is incorporated in the system and the forcing frequency $\Omega = 8$ rad/s is located directly at the right of a resonance peak. Additionally, due to the presence of damping, the nonlinear system exhibits a phase shift compared to the linear system. The amplitude of the motion along the height of the soil column is depicted in Figure 7b. Since the applied Ω is larger than ω_1 of the linear system, the second mode is activated and recall that, to better distinguish the linear solution from the nonlinear one, $\Omega \approx \omega_1$. The second mode can be observed

from this figure due to the presence of almost a zero amplitude in the vicinity of DOF 30. The ratio of softening is presented in Figure 7c and shows a reduction in $G(\gamma)$ with an increase in γ, which is indeed predicted by the hyperbolic soil model (Eq. (4)) and is in accordance with experiments [4]. At the bottom of the soil column, and close to DOF 30, the value of $\Delta\gamma$ is the largest, implying there is the largest reduction due to the presence of the largest shear strains in the soil column. At the top $G^{(N)} = G_0$, hence $\overline{G}_{\text{sec}} = 1$. No reduction of the shear stiffness occur at this location, due to the absence of shear strain, which is also necessary to satisfy the stress-free boundary condition at the surface of the soil column.

Additional insight regarding softening behaviour can be obtained by computing the FRCs of the system, see Figure 8. Directly at the right of the first resonance peak of the linear system ($\omega_1 = 7.41$ rad/s), the amplitude of the motion of the nonlinear system is smaller compared to the linear system, implying softening behaviour. Hence, at the left of the second resonance peak ($\omega_2 = 14.82$ rad/s), the amplitude of the motion of the nonlinear system is larger compared to the linear system, confirming softening behaviour. To check whether unstable branches occur, an upward and downward sweep has been performed. Since no jump occurs, no unstable branches occur, which can also be observed by the fact that the amplitude results of the upward en downward sweep coincide.

For each DOF, the hysteresis loops are presented in Figure 9. The loops reveal the nonlinear and softening character of the column since $\overline{G}_{\text{sec}}$ is not equal to 1 except at the surface as presented in Figure 7. The decrease in $\overline{G}_{\text{sec}}$ implies softening behaviour, which is confirmed by Figure 9. For DOFs in regions at high shear strains, e.g. DOF 30, the hysteresis loops are the largest, implying that the hysteretic damping at these DOFs is also the largest. This is reasonable, since nonlinear hysteretic damping is strain-dependent so larger shear strains will lead to larger hysteretic damping. This is also observed in experiments which have been executed to establish damping curves [4]. Important to note is the nonsmooth transition (C^0 continuity) from the loading to the unloading branch, and vice versa, depicted in Figure 9c. This transition follows from the definition of the Masing rules but is not observed in reality, in particular for course-grained soils. Figure 10, a scatter plot, presents a hysteretic loop at DOF 30. In this figure, the hysteretic loop is plotted as a function of time, in which each dot represents a time sample. Also in this figure, the transition is nonsmooth, because at the transition point there is only one time sample. This implies that a complete stiffness

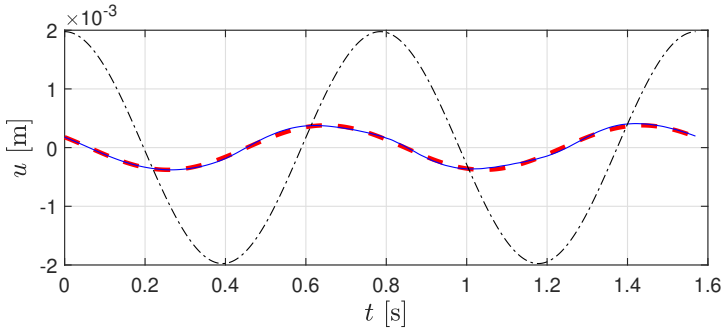

(a) Displacements in the soil column at DOF 30, $z = 40.82$ m, $z_{\mathrm{b}} = 59.18$ m.

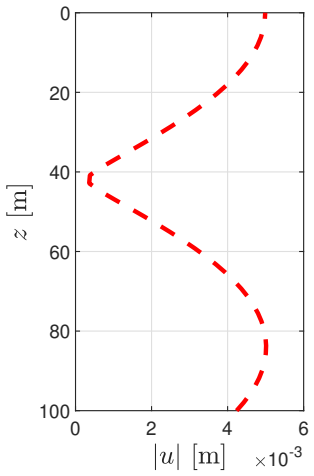

(b) Amplitude.

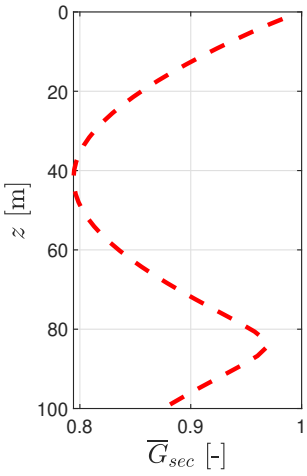

(c) $\overline{G}_{\mathrm{sec}}$.

Figure 7: Displacements in the soil column with nonlinear soil behaviour. (a) Motion at DOF 30. (b) Amplitude of the motion along the soil column. (c) Stiffness reduction along the soil column, expressed in terms of $\overline{G}_{\mathrm{sec}}$. ▪▪▪Motion computed by AFTHBM. -·-·-Motion of the linear system. ——Time-integration results by using ODE45 in MATLAB. Used parameters in this simulation: $H = 100$ m, $N = 50$, $\Omega = 8$ rad/s, $J = 1$, $\gamma_{\mathrm{ref}} = 8.7 \cdot 10^{-4}$, $\beta = 0.91$, $G_0 = 111.86 \cdot 10^6$ N $\cdot$ m^{-2}, $\rho = 2,009.8$ kg $\cdot$m^{-3}, $M = 2^9$, $F_0 = 10,000$ N, $\epsilon = 10^{-9}$.

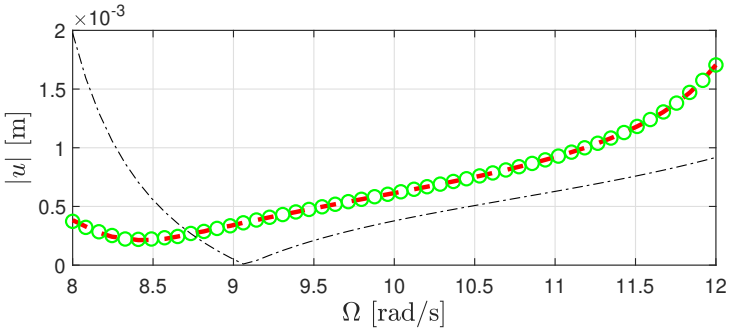

(a) FRC of the nonlinear system at DOF 30, $z = 40.82$ m, $z_b = 59.18$ m.

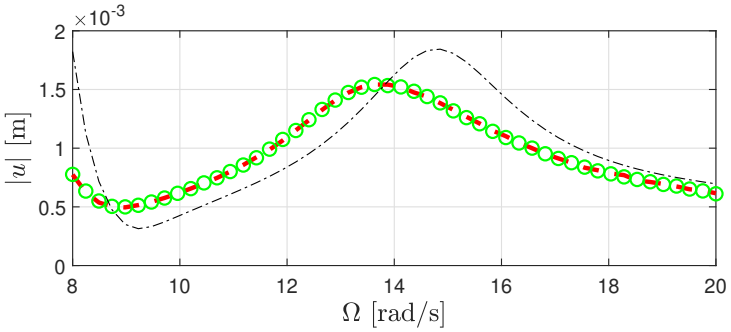

(b) FRC of the nonlinear system at DOF 30, $z = 40.82$ m, $z_b = 59.18$ m. Additional linear viscous damping is applied.

Figure 8: FRCs of the nonlinear system at DOF 30. (a) FRC without additional linear damping. This graph is plotted between the two resonance frequencies of the linear system $\omega_1 = 7.41$ and $\omega_2 = 14.82$ rad/s. (b) FRC including additional linear damping to obtain convergence. This graph is plotted including the second resonance frequency. ▬ Upward frequency sweep. ○ Downward frequency sweep. -·- FRC of the linear system. In the analysis the same parameters have been used as mentioned in Figure 7. In addition, for case (b), a linear viscous damping of $c = 1,500,000$ is applied for all DOFs, on the onset of convergence.

change occurs instantly, which also follows from the Masing rules but is not what is observed in reality.

The nonlinear response is characterised by the occurrence of higher harmonics, which is in correspondence with findings of Zhang et al. [27]. Hence, the simulations are performed again with the same parameters as in Figure 7, but instead $J = 3$, which incorporates the first three harmonics. The single sided spectrum at DOF 30 in Figure 11 contains the amplitude related to the first three harmonics. The amplitude of all the even harmonics should be zero because the result of an integration of an even function over one period yields zero. The odd harmonics decreases when J increases which reveals that for a large amount of harmonics the AFTHBM solution converges to the exact solution, confirming the underlying principle of the HBM. The presence of the higher order harmonics indicates that the behaviour of the soil is indeed nonlinear. The amplitudes of the 0-th and even harmonics are almost zero but not completely due to a limited sampling rate M or a less strict tolerance ϵ. Satisfying a tighter tolerance ϵ is less computational demanding than an increase M. To prevent aliasing, according to the Nyquist sampling theorem, the minimum sampling frequency per period is $2J$ [44]. However, oversampling is in this case better since it increases the accuracy of the solution and will reduce the amplitude coefficients of $\mathbf{a}_0$ almost to zero which is required since the excitation is purely harmonic. Absence of oversampling also causes that even harmonics become more dominant, which is not the case in reality. Moreover, oversampling might be even necessary to have convergence in case of the nonsmooth nonlinear force and need to be considerably higher when higher order harmonics are taken into account. Another reason why oversampling can be necessary is the occurance of ripples in the harmonic approximation of the nonlinear force [7] due to the slow decay of Fourier coefficients, known as the Gibbs-phenomenon. This is especially the case for nonsmooth forces with a low order of continuity. Increasing the number of M will reduce the numerical oscillations causing problems for convergence of the system.

The nonlinear force in the system leads to the introduction of set-valued forces [7, 45], leading to problems in convergence of the system. To partly overcome this problem, is to apply regularization. This implies that the jump in the nonlinear force is smoothed by using a regularization parameter ϵ [33]. The simulations are repeated based on the regularised $\mathbf{f}_{\text{nl}}$, see Eq. (31). For a small regularisation parameter ($\epsilon \approx 10^{-5}$), the results almost coincides with definition of $\mathbf{f}_{\text{nl}}$ based on signum functions but converges closer to resonance

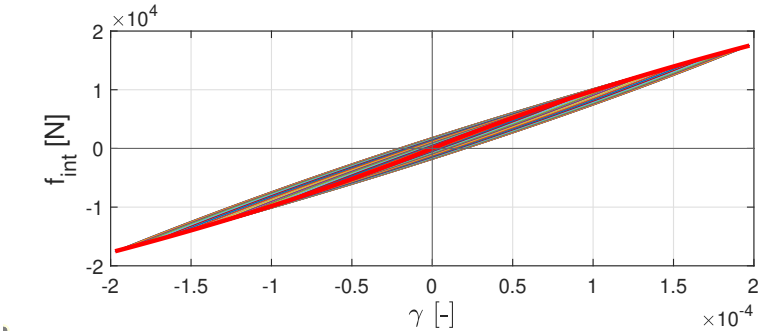

(a) Overview of all the hysteresis loops in the soil column.

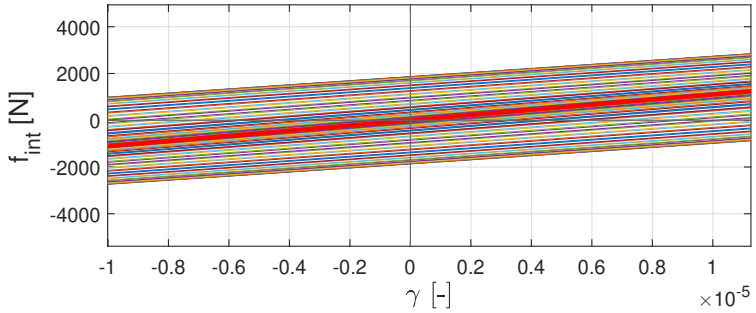

(b) Detail at center of figure (a).

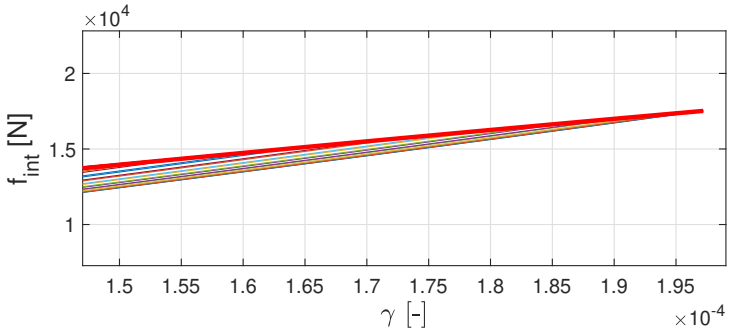

(c) Detail at top right of figure (a).

Figure 9: Hysteresis loops of the soil column with nonlinear behaviour. (a) Overview of all the 49 hysteresis loops. (b) Zoom of the loops at small shear strains. (c) Zoom of the loops at large positive shear strains. —Backbone curve. For the used parameters is referred to Figure 7. Note the degradation of G_{sec}.

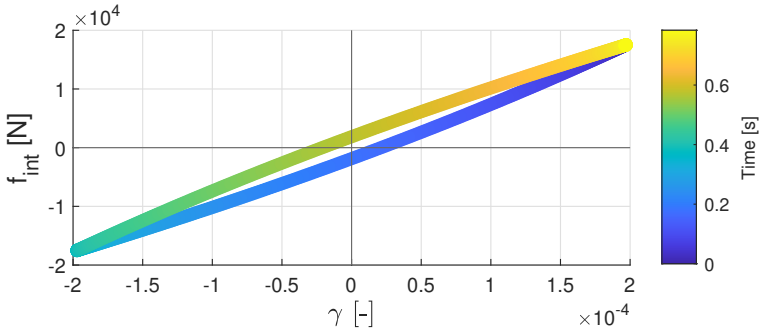

Figure 10: Scatter plot of internal force between DOF $30-31$, which is a specific hysteresis plot (no. 30) of Figure 9 (a). For the simulations the parameters are used as mentioned in Figure 7. The duration of a period T is $2\pi/\Omega = 0.79$ s. After one period a full hysteresis loop is obtained.

frequencies. However, as discussed earlier, the choice of ϵ is not arbitrary and depends on the magnitude of the argument of tanh. For smaller arguments, a smaller ϵ is required to let the solution not drift away from the results based on signum functions and maintaining a sharp transition.

Besides the velocity jumps, the nonsmoothness itself of the nonlinear force can pose difficulties for the Newton-Raphson scheme. Other solution techniques, such as the Broyden method [46] or the Galerkin/Levenberg-Marquardt (GLM) method [17] prove to have better convergence properties.

5. Conclusions and discussion

In this paper, a framework has been presented how nonlinear hysteretic damping can be incorporated in the HBM to obtain the motion of nonlinear soil behaviour, based on the hyperbolic soil model by using the AFTHBM. The method has been applied on a soil column subjected to a prescribed force and a stress-free boundary. In Section 4 multiple analysis have been performed to test the performance of the method and get insight in the nonlinear hysteretic behaviour.

The nonlinear hysteretic damping can be incorporated by using the Masing rules. Hence, the constitutive model does not contain only strain-dependent stiffness but also strain-dependent damping. However, the amplitudes of the cyclic shear strains are unknown a priori and the forces are of a nonsmooth type, requiring an iterative solution procedure which can be well incorporated in the AFTHBM. The nonlinear force can be well treated in the AFTHBM

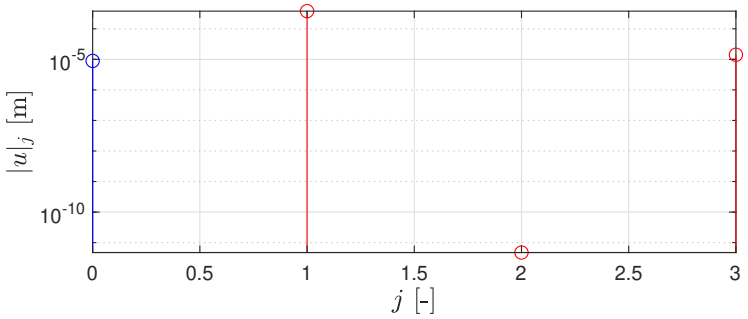

(a) Non-strict tolerance, $\epsilon = 10^{-7}$.

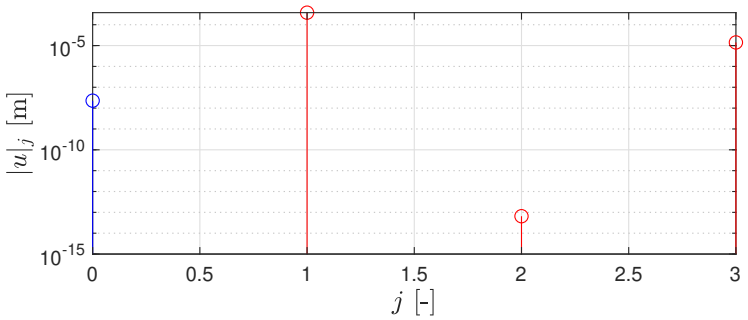

(b) Strict tolerance, $\epsilon = 10^{-9}$.

Figure 11: Spectrum of the first 3 harmonics with $\epsilon = 10^{-7}$ (a) and $\epsilon = 10^{-9}$ (b). The amplitudes for each harmonic j are presented as a function for each harmonic j at DOF 30. ○ 0-th harmonic which is nonzero due to a combination of a limited M and ϵ. ○ Harmonics $1-3$. The odd harmonics and the $0-$th harmonic, related to the rigid body motion, are almost zero for case (b) but clearly nonzero for case (a), emphasizing the importance of setting strict tolerances.

because it is evaluated in the time domain and transformed back into the frequency domain. Also, the iterative solution procedure can be straightforwardly incorporated without the necessity to set up event-driven schemes. To allow the use of AFTHBM, the soil column is discretised by means of a lattice model to a NDOF system.

Results show that the AFTHBM proves to be a good substitute of time-integration methods which take a lot of computational time, especially in this case when the soil model is defined implicitly and thus an iterative procedure is required, leading to incredible long computational times or even when solutions based on time-integration cannot be obtained. To let time-integration results coincide with AFTHBM results, the initial conditions of the time-integration methods needs to be computed very accurately.

Limited sampling can easily lead to wrong results due to accumulated inaccuracies inside the iterative procedure and failing of convergence of the system. Numerical oscillations can be suppressed by increasing the sampling rate. Detection of higher harmonics requires significantly more time samples especially close to resonance frequencies of the system to guarantee convergence of the system. The introduction of smoothing functions slightly improves the performance of the convergence of the system but will not reveal new results.

The nonlinear soil column exhibits softening behaviour, which is represented by smaller amplitudes of the nonlinear system with respect to the linear system, directly at the right of the first resonance peak in the FRC and the degradation of the secant shear stiffness with increasing shear strain, confirming the behaviour as been observed in experiments. Also, for larger shear strains, the hysteretic loops are larger, leading to more dissipated energy at those DOFs. In these hysteretic loops, the transition from the loading to the unloading branch is nonsmooth, but this does not pose problems when implementing the AFTHBM when proper convergence criteria and oversampling is applied. The nonsmoothness is not observed in nature, but follows from the definition of the Masing rules. Employing the AFTHBM on a more smooth material law, like the Bouc-Wen model, would increase the rate of convergence and the computational speed since oversampling is less needed.

To conclude, the AFTHBM is a powerful tool, capable to compute the steady-state response of complex material models including nonlinear hysteretic damping. The models presented in this paper are useful for geotechnical applications but can be extended to other application areas.

Appendix A. Derivation of the analytical derivatives of the hyperbolic soil model

Recall that the partial derivatives of the nonlinear force with respect to the state vectors can be computed like

$$\frac{\partial \mathbf{f}_{\mathrm{nl}}}{\partial \tilde{\mathbf{u}}} = \frac{\partial \mathbf{f}_{\mathrm{nl}}}{\partial \mathbf{u}} \frac{\partial \mathbf{u}}{\partial \tilde{\mathbf{u}}} + \frac{\partial \mathbf{f}_{\mathrm{nl}}}{\partial \dot{\mathbf{u}}} \frac{\partial \dot{\mathbf{u}}}{\partial \tilde{\mathbf{u}}}. \tag{A.1}$$

The derivatives can be expressed in matrix form as follows:

$$\frac{\partial \mathbf{f}_{\mathrm{nl}}}{\partial \mathbf{u}} = \begin{bmatrix} \frac{\partial f_{\mathrm{nl}}^{(1)}}{\partial u^{(1)}} & \frac{\partial f_{\mathrm{nl}}^{(1)}}{\partial u^{(2)}} & \cdots & \frac{\partial f_{\mathrm{nl}}^{(1)}}{\partial u^{(N)}} \\ \frac{\partial f_{\mathrm{nl}}^{(2)}}{\partial u^{(1)}} & \frac{\partial f_{\mathrm{nl}}^{(2)}}{\partial u^{(2)}} & \cdots & \frac{\partial f_{\mathrm{nl}}^{(2)}}{\partial u^{(N)}} \\ \vdots & \vdots & \ddots & \vdots \\ \frac{\partial f_{\mathrm{nl}}^{(N)}}{\partial u^{(1)}} & \frac{\partial f_{\mathrm{nl}}^{(N)}}{\partial u^{(2)}} & \cdots & \frac{\partial f_{\mathrm{nl}}^{(N)}}{\partial u^{(N)}} \end{bmatrix}, \tag{A.2}$$

$$\frac{\partial \mathbf{u}}{\partial \tilde{\mathbf{u}}} = \begin{bmatrix} \frac{\partial u^{(1)}}{\partial c_0^{(1)}} & \cdots & \frac{\partial u^{(1)}}{\partial c_0^{(N)}} & \frac{\partial u^{(1)}}{\partial c_j^{(1)}} & \cdots & \frac{\partial u^{(1)}}{\partial c_j^{(N)}} & \frac{\partial u^{(1)}}{\partial d_j^{(1)}} & \cdots & \frac{\partial u^{(1)}}{\partial d_j^{(N)}} \\ \frac{\partial u^{(2)}}{\partial c_0^{(1)}} & \cdots & \frac{\partial u^{(2)}}{\partial c_0^{(N)}} & \frac{\partial u^{(2)}}{\partial c_j^{(1)}} & \cdots & \frac{\partial u^{(2)}}{\partial c_j^{(N)}} & \frac{\partial u^{(2)}}{\partial d_j^{(1)}} & \cdots & \frac{\partial u^{(2)}}{\partial d_j^{(N)}} \\ \vdots & \ddots & \vdots & \vdots & \ddots & \vdots & \vdots & \ddots & \vdots \\ \frac{\partial u^{(N)}}{\partial c_0^{(1)}} & \cdots & \frac{\partial u^{(N)}}{\partial c_0^{(N)}} & \frac{\partial u^{(N)}}{\partial c_j^{(1)}} & \cdots & \frac{\partial u^{(N)}}{\partial c_j^{(N)}} & \frac{\partial u^{(N)}}{\partial d_j^{(1)}} & \cdots & \frac{\partial u^{(N)}}{\partial d_j^{(N)}} \end{bmatrix},$$

$$\frac{\partial \mathbf{f}_{\mathrm{nl}}}{\partial \dot{\mathbf{u}}} = \begin{bmatrix} \frac{\partial f_{\mathrm{nl}}^{(1)}}{\partial \dot{u}^{(1)}} & \frac{\partial f_{\mathrm{nl}}^{(1)}}{\partial \dot{u}^{(2)}} & \cdots & \frac{\partial f_{\mathrm{nl}}^{(1)}}{\partial \dot{u}^{(N)}} \\ \frac{\partial f_{\mathrm{nl}}^{(2)}}{\partial \dot{u}^{(1)}} & \frac{\partial f_{\mathrm{nl}}^{(2)}}{\partial \dot{u}^{(2)}} & \cdots & \frac{\partial f_{\mathrm{nl}}^{(2)}}{\partial \dot{u}^{(N)}} \\ \vdots & \vdots & \ddots & \vdots \\ \frac{\partial f_{\mathrm{nl}}^{(N)}}{\partial \dot{u}^{(1)}} & \frac{\partial f_{\mathrm{nl}}^{(N)}}{\partial \dot{u}^{(2)}} & \cdots & \frac{\partial f_{\mathrm{nl}}^{(N)}}{\partial \dot{u}^{(N)}} \end{bmatrix},$$

$$\frac{\partial \dot{\mathbf{u}}}{\partial \tilde{\mathbf{u}}} = \begin{bmatrix} \frac{\partial \dot{u}^{(1)}}{\partial c_0^{(1)}} & \cdots & \frac{\partial \dot{u}^{(1)}}{\partial c_0^{(N)}} & \frac{\partial \dot{u}^{(1)}}{\partial c_j^{(1)}} & \cdots & \frac{\partial \dot{u}^{(1)}}{\partial c_j^{(N)}} & \frac{\partial \dot{u}^{(1)}}{\partial d_j^{(1)}} & \cdots & \frac{\partial \dot{u}^{(1)}}{\partial d_j^{(N)}} \\ \frac{\partial \dot{u}^{(2)}}{\partial c_0^{(1)}} & \cdots & \frac{\partial \dot{u}^{(2)}}{\partial c_0^{(N)}} & \frac{\partial \dot{u}^{(2)}}{\partial c_j^{(1)}} & \cdots & \frac{\partial \dot{u}^{(2)}}{\partial c_j^{(N)}} & \frac{\partial \dot{u}^{(2)}}{\partial d_j^{(1)}} & \cdots & \frac{\partial \dot{u}^{(2)}}{\partial d_j^{(N)}} \\ \vdots & \ddots & \vdots & \vdots & \ddots & \vdots & \vdots & \ddots & \vdots \\ \frac{\partial \dot{u}^{(N)}}{\partial c_0^{(1)}} & \cdots & \frac{\partial \dot{u}^{(N)}}{\partial c_0^{(N)}} & \frac{\partial \dot{u}^{(N)}}{\partial c_j^{(1)}} & \cdots & \frac{\partial \dot{u}^{(N)}}{\partial c_j^{(N)}} & \frac{\partial \dot{u}^{(N)}}{\partial d_j^{(1)}} & \cdots & \frac{\partial \dot{u}^{(N)}}{\partial d_j^{(N)}} \end{bmatrix}. \tag{A.3}$$

Appendix A.1. Non-regularised nonlinear force definition

Appendix A.1.1. Terms of $\partial \mathbf{f}_{nl}/\partial \mathbf{u}$

$$A^{(1)} = \frac{\left|\gamma^{(1)} + B^{(1)}\right|}{2\gamma_{\text{ref}}} \quad , \quad B^{(1)} = \text{sgn}\left(\dot{\gamma}^{(1)}\right)\Delta\gamma^{(1)}$$

$$\frac{\partial f_{\text{nl}}^{(1)}}{\partial u^{(1)}} = \frac{G_0}{\Delta z\left[1+\left(A^{(1)}\right)^{\beta}\right]} - \left[G_0\left(\gamma^{(1)}+B^{(1)}\right)\left(A^{(1)}\right)^{\beta}\beta\,\text{sgn}\left(\gamma^{(1)}+B^{(1)}\right)\right] \Big/ \left\{\left[1+\left(A^{(1)}\right)^{\beta}\right]^2 \Delta z\left|\gamma^{(1)}+B^{(1)}\right|\right\} \tag{A.4}$$

$$\frac{\partial f_{\text{nl}}^{(1)}}{\partial u^{(2)}} = -\frac{\partial f_{\text{nl}}^{(1)}}{\partial u^{(1)}}$$

$$A^{(N-1)} = \frac{\left|\gamma^{(N-1)} + B^{(N-1)}\right|}{2\gamma_{\text{ref}}} \quad , \quad B^{(N-1)} = \text{sgn}\left(\dot{\gamma}^{(N-1)}\right)\Delta\gamma^{(N-1)}$$

$$\frac{\partial f_{\text{nl}}^{(N)}}{\partial u^{(N-1)}} = \frac{G_0}{\Delta z\left[1+\left(A^{(N-1)}\right)^{\beta}\right]} - \left[G_0\left(\gamma^{(N-1)}+B^{(N-1)}\right)\left(A^{(N-1)}\right)^{\beta}\beta\,\text{sgn}\left(\gamma^{(N-1)}+B^{(N-1)}\right)\right] \Big/ \left\{\left[1+\left(A^{(N-1)}\right)^{\beta}\right]^2 \Delta z\left|\gamma^{(N-1)}+B^{(N-1)}\right|\right\}$$

$$\frac{\partial f_{\text{nl}}^{(N)}}{\partial u^{(N)}} = -\frac{\partial f_{\text{nl}}^{(N)}}{\partial u^{(N-1)}}$$

$$A^{(\alpha)} = \frac{\left|\gamma^{(\alpha)} + B^{(\alpha)}\right|}{2\gamma_{\text{ref}}} \quad , \quad B^{(\alpha)} = \text{sgn}\left(\dot{\gamma}^{(\alpha)}\right) \Delta\gamma^{(\alpha)}$$

$$\frac{\partial f_{\text{nl}}^{(i)}}{\partial u^{(\alpha)}} = -\frac{G_0}{\Delta z \left[1 + \left(A^{(\alpha)}\right)^{\beta}\right]} + \left[G_0 \left(\gamma^{(\alpha)} + B^{(\alpha)}\right) \left(A^{(\alpha)}\right)^{\beta} \beta \, \text{sgn}\left(\gamma^{(\alpha)} + B^{(\alpha)}\right)\right] \Bigg/ \left\{\left[1 + \left(A^{(\alpha)}\right)^{\beta}\right]^2 \Delta z \left|\gamma^{(\alpha)} + B^{(\alpha)}\right|\right\} \tag{A.5}$$

$$A^{(\alpha)} = \frac{\left|\gamma^{(\alpha)} + B^{(\alpha)}\right|}{2\gamma_{\text{ref}}} \quad , \quad B^{(\alpha)} = \text{sgn}\left(\dot{\gamma}^{(\alpha)}\right) \Delta\gamma^{(\alpha)}$$

$$\frac{\partial f_{\text{nl}}^{(i)}}{\partial u^{(i+1)}} = -\frac{G_0}{\Delta z \left[1 + \left(A^{(\alpha)}\right)^{\beta}\right]} + \left[G_0 \left(\gamma^{(\alpha)} + B^{(\alpha)}\right) \left(A^{(\alpha)}\right)^{\beta} \beta \, \text{sgn}\left(\gamma^{(\alpha)} + B^{(\alpha)}\right)\right] \Bigg/ \left\{\left[1 + \left(A^{(\alpha)}\right)^{\beta}\right]^2 \Delta z \left|\gamma^{(\alpha)} + B^{(\alpha)}\right|\right\}$$

$$\frac{\partial f_{\text{nl}}^{(i)}}{\partial u^{(i)}} = -\frac{\partial f_{\text{nl}}^{(i)}}{\partial u^{(i-1)}} - \frac{\partial f_{\text{nl}}^{(i)}}{\partial u^{(i+1)}} \tag{A.6}$$

Appendix A.1.2. Terms of $\partial\mathbf{u}/\partial\tilde{\mathbf{u}}$

$$\frac{\partial u^{(i)}}{\partial c_0^{(k)}} = \delta_{i,k} \tag{A.7}$$

$$\frac{\partial u^{(i)}}{\partial c_j^{(k)}} = \delta_{i,k} \cos\left(j\Omega t\right)$$

$$\frac{\partial u^{(i)}}{\partial d_j^{(k)}} = \delta_{i,k} \sin\left(j\Omega t\right) \tag{A.8}$$

Where in (A.11)

$$\delta_{i,k} = \begin{cases} 1 & \text{if} \quad i = k \\ 0 & \text{otherwise} \end{cases} \tag{A.9}$$

is the Kronecker delta.

Appendix A.1.3. Terms of $\partial \mathbf{f}_{nl}/\partial \dot{\mathbf{u}}$

$$A^{(1)} = \frac{\left|\gamma^{(1)} + B^{(1)}\right|}{2\gamma_{\text{ref}}} \quad , \quad B^{(1)} = \text{sgn}\left(\dot{\gamma}^{(1)}\right)\Delta\gamma^{(1)}$$

$$\frac{\partial f_{\text{nl}}^{(1)}}{\partial \dot{u}^{(1)}} = -\frac{2G_0\delta\left(\dot{\gamma}^{1)}\right)\Delta\gamma^{(1)}}{\left[1+\left(A^{(1)}\right)^{\beta}\right]} +$$

$$\left\{G_0\left[\gamma^{(1)}+B^{(1)}\right]\left(A^{(1)}\right)^{\beta}\beta B^{(1)}2\delta\left(\dot{\gamma}^{(1)}\right)\Delta\gamma^{(1)}\,\text{sgn}\left(\gamma^{(1)}+B^{(1)}\right)\right\} \Big/$$

$$\left\{\left[1+\left(A^{(1)}\right)^{\beta}\right]^2\left|\gamma^{(1)}+B^{(1)}\right|\right\} + \frac{2G_0\delta\left(\dot{\gamma}^{(1)}\right)\Delta\gamma^{(1)}}{1+\left(\dfrac{\Delta\gamma^{(1)}}{\gamma_{\text{ref}}}\right)^{\beta}}$$

$$\frac{\partial f_{\text{nl}}^{(1)}}{\partial \dot{u}^{(2)}} = \frac{\partial f_{\text{nl}}^{(1)}}{\partial \dot{u}^{(1)}}$$

$$A^{(N-1)} = \frac{\left|\gamma^{(N-1)} + B^{(N-1)}\right|}{2\gamma_{\text{ref}}} \quad , \quad B^{(N-1)} = \text{sgn}\left(\dot{\gamma}^{(N-1)}\right)\Delta\gamma^{(N-1)}$$

$$\frac{\partial f_{\text{nl}}^{(N)}}{\partial \dot{u}^{(N-1)}} = -\frac{2G_0\delta\left(\dot{\gamma}^{N-1)}\right)\Delta\gamma^{(N-1)}}{\left[1+\left(A^{(N-1)}\right)^{\beta}\right]} +$$

$$\left\{G_0\left[\gamma^{(N-1)}+B^{(N-1)}\right]\left(A^{(N-1)}\right)^{\beta}\beta B^{(N-1)}2\delta\left(\dot{\gamma}^{(N-1)}\right)\right.$$

$$\left.\Delta\gamma^{(N-1)}\,\text{sgn}\left(\gamma^{(N-1)}+B^{(N-1)}\right)\right\} \Big/$$

$$\left\{\left[1+\left(A^{(N-1)}\right)^{\beta}\right]^2\left|\gamma^{(N-1)}+B^{(N-1)}\right|\right\} + \frac{2G_0\delta\left(\dot{\gamma}^{(N-1)}\right)\Delta\gamma^{(N-1)}}{1+\left(\dfrac{\Delta\gamma^{(N-1)}}{\gamma_{\text{ref}}}\right)^{\beta}}$$

$$\frac{\partial f_{\text{nl}}^{(N)}}{\partial \dot{u}^{(N)}} = \frac{\partial f_{\text{nl}}^{(N)}}{\partial \dot{u}^{(N-1)}}$$

$$A^{(\alpha)} = \frac{\left|\gamma^{(\alpha)} + B^{(\alpha)}\right|}{2\gamma_{\text{ref}}} \quad , \quad B^{(\alpha)} = \text{sgn}\left(\dot{\gamma}^{(\alpha)}\right)\Delta\gamma^{(\alpha)}$$

$$\frac{\partial f_{\text{nl}}^{(i)}}{\partial \dot{u}^{(i-1)}} = -\frac{2G_0\delta\left(\dot{\gamma}^{\alpha)}\right)\Delta\gamma^{(\alpha)}}{\left[1+\left(A^{(\alpha)}\right)^{\beta}\right]} +$$

$$\left\{G_0\left[\gamma^{(\alpha)} + B^{(\alpha)}\right]\left(A^{(\alpha)}\right)^{\beta}\beta B^{(i-1,i)} 2\delta\left(\dot{\gamma}^{(\alpha)}\right)\right.$$

$$\left.\Delta\gamma^{(\alpha)}\,\text{sgn}\left(\gamma^{(\alpha)} + B^{(\alpha)}\right)\right\} \Big/$$

$$\left\{\left[1+\left(A^{(\alpha)}\right)^{\beta}\right]^2\left|\gamma^{(\alpha)} + B^{(\alpha)}\right|\right\} + \frac{2G_0\delta\left(\dot{\gamma}^{(\alpha)}\right)\Delta\gamma^{(\alpha)}}{1+\left(\dfrac{\Delta\gamma^{(\alpha)}}{\gamma_{\text{ref}}}\right)^{\beta}}$$

$$A^{(\alpha)} = \frac{\left|\gamma^{(\alpha)} + B^{(\alpha)}\right|}{2\gamma_{\text{ref}}} \quad , \quad B^{(\alpha)} = \text{sgn}\left(\dot{\gamma}^{(\alpha)}\right)\Delta\gamma^{(\alpha)} \tag{A.10}$$

$$\frac{\partial f_{\text{nl}}^{(i)}}{\partial \dot{u}^{(i+1)}} = -\frac{2G_0\delta\left(\dot{\gamma}^{(\alpha)}\right)\Delta\gamma^{(\alpha)}}{\left[1+\left(A^{(\alpha)}\right)^{\beta}\right]} +$$

$$\left\{G_0\left[\gamma^{(\alpha)} + B^{(\alpha)}\right]\left(A^{(\alpha)}\right)^{\beta}\beta B^{(\alpha)} 2\delta\left(\dot{\gamma}^{(\alpha)}\right)\right.$$

$$\left.\Delta\gamma^{(\alpha)}\,\text{sgn}\left(\gamma^{(\alpha)} + B^{(\alpha)}\right)\right\} \Big/$$

$$\left\{\left[1+\left(A^{(\alpha)}\right)^{\beta}\right]^2\left|\gamma^{(\alpha)} + B^{(\alpha)}\right|\right\} + \frac{2G_0\delta\left(\dot{\gamma}^{(\alpha)}\right)\Delta\gamma^{(\alpha)}}{1+\left(\dfrac{\Delta\gamma^{(\alpha)}}{\gamma_{\text{ref}}}\right)^{\beta}}$$

$$\frac{\partial f_{\text{nl}}^{(i)}}{\partial \dot{u}^{(i)}} = -\frac{\partial f_{\text{nl}}^{(i)}}{\partial \dot{u}^{(i-1)}} + \frac{\partial f_{\text{nl}}^{(i)}}{\partial \dot{u}^{(i+1)}}$$

Appendix A.1.4. Terms of $\partial\dot{\mathbf{u}}/\partial\tilde{\mathbf{u}}$

$$\frac{\partial \dot{u}^{(i)}}{\partial c_0^{(k)}} = 0 \tag{A.11}$$

$$\frac{\partial \dot{u}^{(i)}}{\partial c_j^{(k)}} = -\delta_{i,k} j\Omega \sin\left(j\Omega t\right)$$

$$\frac{\partial \dot{u}^{(i)}}{\partial d_j^{(k)}} = \delta_{i,k} j\Omega \cos\left(j\Omega t\right) \tag{A.12}$$

Appendix A.2. Regularised nonlinear force definition

Appendix A.2.1. Terms of $\partial \mathbf{f}_{nl}/\partial \mathbf{u}$

$$A^{(1)} = \frac{\gamma^{(1)} + B^{(1)}}{2\gamma_{\text{ref}}} \quad , \quad B^{(1)} = \tanh\left(\dot{\gamma}^{(1)}/\varepsilon\right)\Delta\gamma^{(1)}$$

$$\frac{\partial f_{\text{nl}}^{(1)}}{\partial u^{(1)}} = \frac{G_0}{\Delta z\left[1+\left(A^{(1)}\right)^{\beta}\right]} - \left[G_0\left(\gamma^{(1)}+B^{(1)}\right)\left(A^{(1)}\right)^{\beta}\beta\,\text{sgn}\left(\gamma^{(1)}+B^{(1)}\right)\right] \Big/ \left\{\left[1+\left(A^{(1)}\right)^{\beta}\right]^2 \Delta z\left|\gamma^{(1)}+B^{(1)}\right|\right\}$$

$$\frac{\partial f_{\text{nl}}^{(1)}}{\partial u^{(2)}} = -\frac{\partial f_{\text{nl}}^{(1)}}{\partial u^{(1)}}$$

$$A^{(N-1,N)} = \frac{\left|\gamma^{(N-1)} + B^{(N-1)}\right|}{2\gamma_{\text{ref}}} \quad , \quad B^{(N-1)} = \tanh\left(\dot{\gamma}^{(N-1)}/\varepsilon\right)\Delta\gamma^{(N-1)}$$

$$\frac{\partial f_{\text{nl}}^{(N)}}{\partial u^{(N-1)}} = \frac{G_0}{\Delta z\left[1+\left(A^{(N-1)}\right)^{\beta}\right]} - , \left[G_0\left(\gamma^{(N-1)}+B^{(N-1)}\right)\left(A^{(N-1)}\right)^{\beta}\beta\,\text{sgn}\left(\gamma^{(N-1)}+B^{(N-1)}\right)\right] \Big/ \left\{\left[1+\left(A^{(N-1)}\right)^{\beta}\right]^2 \Delta z\left|\gamma^{(N-1)}+B^{(N-1)}\right|\right\}$$

$$\frac{\partial f_{\text{nl}}^{(N)}}{\partial u^{(N)}} = -\frac{\partial f_{\text{nl}}^{(N)}}{\partial u^{(N-1)}}$$

$$A^{(\alpha)} = \frac{\left|\gamma^{(\alpha)} + B^{(\alpha)}\right|}{2\gamma_{\text{ref}}} \quad , \quad B^{(\alpha)} = \tanh\left(\dot{\gamma}^{(\alpha)}/\varepsilon\right)\Delta\gamma^{(\alpha)}$$

$$\frac{\partial f_{\text{nl}}^{(i)}}{\partial u^{(i-1)}} = -\frac{G_0}{\Delta z\left[1 + \left(A^{(\alpha)}\right)^{\beta}\right]} + \left[G_0\left(\gamma^{(\alpha)} + B^{(\alpha)}\right)\left(A^{(\alpha)}\right)^{\beta}\beta\,\text{sgn}\left(\gamma^{(\alpha)} + B^{(\alpha)}\right)\right] \Big/ \left\{\left[1 + \left(A^{(\alpha)}\right)^{\beta}\right]^2 \Delta z\left|\gamma^{(\alpha)} + B^{(\alpha)}\right|\right\} \tag{A.13}$$

$$A^{(\alpha)} = \frac{\left|\gamma^{(\alpha)} + B^{(\alpha)}\right|}{2\gamma_{\text{ref}}} \quad , \quad B^{(\alpha)} = \tanh\left(\dot{\gamma}^{(\alpha)}/\varepsilon\right)\Delta\gamma^{(\alpha)}$$

$$\frac{\partial f_{\text{nl}}^{(i)}}{\partial u^{(i+1)}} = -\frac{G_0}{\Delta z\left[1 + \left(A^{\alpha}\right)^{\beta}\right]} + \left[G_0\left(\gamma^{(\alpha)} + B^{(\alpha)}\right)\left(A^{(\alpha)}\right)^{\beta}\beta\,\text{sgn}\left(\gamma^{(\alpha)} + B^{(\alpha)}\right)\right] \Big/ \left\{\left[1 + \left(A^{(\alpha)}\right)^{\beta}\right]^2 \Delta z\left|\gamma^{(\alpha)} + B^{(\alpha)}\right|\right\}$$

$$\frac{\partial f_{\text{nl}}^{(i)}}{\partial u^{(i)}} = -\frac{\partial f_{\text{nl}}^{(i)}}{\partial u^{(i-1)}} - \frac{\partial f_{\text{nl}}^{(i)}}{\partial u^{(i+1)}} \tag{A.14}$$

Appendix A.2.2. Terms of $\partial\mathbf{u}/\partial\tilde{\mathbf{u}}$

For the partial derivatives $\partial\mathbf{u}/\partial\tilde{\mathbf{u}}$ is referred to subsection Appendix A.1.2.

Appendix A.2.3. Terms of $\partial\mathbf{f}_{nl}/\partial\dot{\mathbf{u}}$

$$A^{(1)} = \frac{\gamma^{(1)} + B^{(1)}}{2\gamma_{\text{ref}}} \quad , \quad B^{(1)} = \tanh\left(\dot{\gamma}^{(1)}/\varepsilon\right)\Delta\gamma^{(1)} \quad ,$$

$$C^{(1)} = 1 - \tanh\left(\dot{\gamma}^{(1)}/\ \varepsilon\right)^2$$

$$\frac{\partial f_{\text{nl}}^{(1)}}{\partial \dot{u}^{(1)}} = \frac{G_0 C^{(1)}\Delta\gamma^{(1)}}{\Delta z\left[1 + \left(A^{(1)}\right)^{\beta}\right]} -$$

$$\left\{G_0\Delta\gamma^{(1)}\left(\gamma^{(1)} + B^{(1)}\right)\left(A^{(1)}\right)^{\beta}\beta C^{(1)}\,\text{sgn}\left(\gamma^{(1)} + B^{(1)}\right)\right\} \Big/$$

$$\left\{\left[1 + \left(A^{(1)}\right)^{\beta}\right]^2 \Delta z\ \varepsilon\left|\gamma^{(1)} + B^{(1)}\right|\right\} - \frac{G_0\Delta\gamma^{(1)}C^{(1)}}{\Delta z\ \varepsilon\left[\left(1 + \dfrac{\Delta\gamma^{(1)}}{\gamma_{\text{ref}}}\right)^{\beta}\right]}$$

$$\frac{\partial f_{\text{nl}}^{(1)}}{\partial \dot{u}^{(2)}} = -\frac{\partial f_{\text{nl}}^{(1)}}{\partial \dot{u}^{(1)}}$$

$$A^{(N-1)} = \frac{\gamma^{(N-1)} + B^{(N-1)}}{2\gamma_{\text{ref}}} \quad , \quad B^{(N-1)} = \tanh\left(\dot{\gamma}^{(N-1)}/\varepsilon\right) \Delta\gamma^{(N-1)} \quad ,$$

$$C^{(N-1)} = 1 - \tanh\left(\dot{\gamma}^{(N-1)}/\ \varepsilon\right)^2$$

$$\frac{\partial f_{\text{nl}}^{(N)}}{\partial \dot{u}^{(N-1)}} = -\frac{G_0 C^{(N-1)} \Delta\gamma^{(N-1)}}{\Delta z \left[1 + \left(A^{(N-1)}\right)^{\beta}\right]} +$$

$$\left\{G_0 \Delta\gamma^{(N-1)} \left(\gamma^{(N-1)} + B^{(N-1)}\right) \left(A^{(N-1)}\right)^{\beta} \beta C^{(N-1)} \operatorname{sgn}\left(\gamma^{(N-1)} + B^{(N-1)}\right)\right\} \Big/$$

$$\left\{\left[1 + \left(A^{(N-1)}\right)^{\beta}\right]^2 \Delta z\ \varepsilon \left|\gamma^{(N-1)} + B^{(N-1)}\right|\right\} + \frac{G_0 \Delta\gamma^{(N-1)} C^{(N-1)}}{\Delta z\ \varepsilon \left[\left(1 + \dfrac{\Delta\gamma^{(N-1)}}{\gamma_{\text{ref}}}\right)^{\beta}\right]}$$

$$\frac{\partial f_{\text{nl}}^{(N)}}{\partial \dot{u}^{(N)}} = -\frac{\partial f_{\text{nl}}^{(N)}}{\partial \dot{u}^{(N-1)}}$$

$$A^{(\alpha)} = \frac{\gamma^{(\alpha)} + B^{(\alpha)}}{2\gamma_{\text{ref}}} \quad , \quad B^{(\alpha)} = \tanh\left(\dot{\gamma}^{(\alpha)}/\varepsilon\right)\Delta\gamma^{(\alpha)} \quad ,$$

$$C^{(\alpha)} = 1 - \tanh\left(\dot{\gamma}^{(\alpha)}/\ \varepsilon\right)^2$$

$$\frac{\partial f_{\text{nl}}^{(i)}}{\partial \dot{u}^{(i-1)}} = -\frac{G_0 C^{(\alpha)}\Delta\gamma^{(\alpha)}}{\Delta z\left[1 + \left(A^{(\alpha)}\right)^{\beta}\right]} +$$

$$\left\{G_0\Delta\gamma^{(\alpha)}\left(\gamma^{(\alpha)} + B^{(\alpha)}\right)\left(A^{(\alpha)}\right)^{\beta}\beta C^{(\alpha)}\,\text{sgn}\left(\gamma^{(\alpha)} + B^{(\alpha)}\right)\right\} \Big/$$

$$\left\{\left[1 + \left(A^{(\alpha)}\right)^{\beta}\right]^2 \Delta z\ \varepsilon\left|\gamma^{(\alpha)} + B^{(\alpha)}\right|\right\} + \frac{G_0\Delta\gamma^{(\alpha)}C^{(\alpha)}}{\Delta z\ \varepsilon\left[\left(1 + \dfrac{\Delta\gamma^{(\alpha)}}{\gamma_{\text{ref}}}\right)^{\beta}\right]}$$

$$A^{(\alpha)} = \frac{\gamma^{(\alpha)} + B^{(\alpha)}}{2\gamma_{\text{ref}}} \quad , \quad B^{(\alpha)} = \tanh\left(\dot{\gamma}^{(\alpha)}/\varepsilon\right)\Delta\gamma^{(\alpha)} \quad ,$$

$$C^{(\alpha)} = 1 - \tanh\left(\dot{\gamma}^{(\alpha)}/\ \varepsilon\right)^2$$

$$\frac{\partial f_{\text{nl}}^{(i)}}{\partial \dot{u}^{(i+1)}} = -\frac{G_0 C^{(\alpha)}\Delta\gamma^{(\alpha)}}{\Delta z\left[1 + \left(A^{(\alpha)}\right)^{\beta}\right]} +$$

$$\left\{G_0\Delta\gamma^{(\alpha)}\left(\gamma^{(\alpha)} + B^{(\alpha)}\right)\left(A^{(\alpha)}\right)^{\beta}\beta C^{(\alpha)}\,\text{sgn}\left(\gamma^{(\alpha)} + B^{(\alpha)}\right)\right\} \Big/$$

$$\left\{\left[1 + \left(A^{(\alpha)}\right)^{\beta}\right]^2 \Delta z\ \varepsilon\left|\gamma^{(\alpha)} + B^{(\alpha)}\right|\right\} + \frac{G_0\Delta\gamma^{(\alpha)}C^{(\alpha)}}{\Delta z\ \varepsilon\left[\left(1 + \dfrac{\Delta\gamma^{(\alpha)}}{\gamma_{\text{ref}}}\right)^{\beta}\right]}$$

$$\frac{\partial f_{\text{nl}}^{(i)}}{\partial \dot{u}^{(i)}} = -\frac{\partial f_{\text{nl}}^{(i)}}{\partial \dot{u}^{(i-1)}} - \frac{\partial f_{\text{nl}}^{(i)}}{\partial \dot{u}^{(i+1)}} \tag{A.15}$$

Appendix A.2.4. Terms of $\partial\dot{\mathbf{u}}/\partial\tilde{\mathbf{u}}$

For the partial derivatives $\partial\dot{\mathbf{u}}/\partial\tilde{\mathbf{u}}$ is referred to subsection A.11.

Appendix B. Implementation of the Bouc-Wen model of hysteresis

Appendix B.1. Introduction

The Bouc-Wen model of hysteresis is a nonlinear hysteretic material model, often applied for modelling isolators, metals, magnetism, structures and other applications [17, 39, 47]. On the contrary of Masing type hysteresis, the Bouc-Wen model is able to include a more smooth transition between the loading and the unloading branch. The model is capable to describe hysteretic behaviour based on the transition from the elastic to the plastic branch, hence capable of capturing post-yielding behaviour. Likewise the Masing rules, the AFTHBM is employed to solve the Bouc-Wen model applied to a NDOF system.

Appendix B.2. Equations of motion

For a SDOF system, the constitutive model can be described by the nonlinear differential equation [17]

$$\dot{z} = \dot{u}\{\kappa - [\gamma_\mathrm{b} + \beta_\mathrm{b}\,\mathrm{sgn}\,(\dot{u})\,\mathrm{sgn}\,(z)]\,|z|^n\}, \tag{B.1}$$

where z denotes the nonlinear hysteretic displacement in m, u the response of the system in m and κ, γ_b, β_b and n are dimensionless parameters which determine the shape of the hysteresis loops [25, 48]. All the parameters are positive, except for γ_b which can be either positive or negative [49]. Higher values of n increases the sharpness of the transition zones between the branches and higher values of β_b produces fatter loops, controls the stiffness change when the sign of $\dot{u}$ is changing, and κ governs the slope of the hysteresis loops at zero hysteretic displacement [17, 39]. Softening of the system occurs if $\gamma_\mathrm{b} + \beta_\mathrm{b} > 0$, hardening if $\gamma_\mathrm{b} + \beta_\mathrm{b} < 0$. Incorporating the Bouc-Wen element in the system, the governing equation of motion turns into

$$m\ddot{u} + k_\mathrm{r}\alpha u + k_\mathrm{r}\,(1-\alpha)\,z = F_\mathrm{ext}, \tag{B.2}$$

where m is the mass of the system, α the stiffness ratio [39] and k_r the restoring spring stiffness, all excited by an external force F_ext. α is given by

$$\alpha = \frac{k_\mathrm{p}}{k_\mathrm{r}}, \tag{B.3}$$

where k_p is the post-yield stiffness and k_r the pre-yield stiffness. The nonlinear force in Eq. (B.2), which is the hysteretic component of the restoring force, is given by

$$k_\mathrm{r}\left(1-\alpha\right)z. \tag{B.4}$$

Important to note is that neither viscous damping nor additional linear stiffness is present, all the damping is assumed to be hysteretic and incorporated in the Bouc-Wen model. For a NDOF system, the governing set of equations in the time domain is given by

$$\mathbf{M}\ddot{\mathbf{u}} + \mathbf{K}_\mathrm{elas}\mathbf{u} + \mathbf{K}_\mathrm{hyst}\mathbf{z} = \mathbf{F}_\mathrm{ext}, \tag{B.5}$$

where $\mathbf{M}$, $\mathbf{C}$ and $\mathbf{K}$ are the mass, damping and spring matrices respectively, $\mathbf{K}_\mathrm{elas}$ the matrix containing the elastic restoring force, $\mathbf{K}_\mathrm{hyst}$ the matrix containing the matrix with the hysteretic restoring force and $\mathbf{F}_\mathrm{ext}$ a vector containing the external forces. The motion and its derivatives are given by

$$\mathbf{u} = \mathbf{a_0} + \sum_{j=1}^{J}\left[\mathbf{a}_j\cos\left(j\Omega t\right) + \mathbf{b}_j\sin\left(j\Omega t\right)\right], \tag{B.6}$$

$$\dot{\mathbf{u}} = \sum_{j=1}^{J}\left[-\mathbf{a}_j j\Omega\sin\left(j\Omega t\right) + \mathbf{b}_j j\Omega\cos\left(j\Omega t\right)\right], \tag{B.7}$$

$$\ddot{\mathbf{u}} = \sum_{j=1}^{J}\left[-\mathbf{a}_j j^2\Omega^2\cos\left(j\Omega t\right) - \mathbf{b}_j j^2\Omega^2\sin\left(j\Omega t\right)\right]. \tag{B.8}$$

Since the Bouc-Wen model is described by a nonlinear differential equation, it is not possible to write the nonlinear hysteretic displacement $\mathbf{z}$ explictly as a function of $\mathbf{u}$. Hence, one has two unknown vectors, namely $\tilde{\mathbf{u}}$ and $\tilde{\mathbf{z}}$, in which the latter contains the unknown Fourier expansion coefficients of the hysteretic force. Expressing $\tilde{\mathbf{z}}$ in terms of $\tilde{\mathbf{q}}$ and applying a Galerkin procedure [17], the system can be solved. Rewriting Eq. (B.5) in the frequency domain yields

$$\hat{\mathbf{M}}\hat{\mathbf{D}}\hat{\mathbf{D}}\tilde{\mathbf{u}} + \hat{\mathbf{K}}_\mathrm{elas}\tilde{\mathbf{u}} + \hat{\mathbf{K}}_\mathrm{hyst}\tilde{\mathbf{z}} = \hat{\mathbf{F}}_\mathrm{ext}, \tag{B.9}$$

where the $\hat{}$ denotes the partitioned matrix of either $\mathbf{M}$, $\mathbf{C}$ or $\mathbf{K}$. Hence $\hat{\mathbf{M}}$, $\hat{\mathbf{K}}_{\text{elas}}$, $\hat{\mathbf{K}}_{\text{hyst}}$ and $\hat{\mathbf{F}}_{\text{ext}}$ are given by

$$\hat{\mathbf{M}} = \begin{bmatrix} \mathbf{M}^{(0)} & & \\ & \ddots & \\ & & \mathbf{M}^{(2J+1)} \end{bmatrix} \quad , \quad \mathbf{M}^{(a)} = \begin{bmatrix} m_1 & 0 & 0 & \cdots & 0 \\ 0 & m_2 & 0 & & 0 \\ 0 & \ddots & \ddots & \ddots & \vdots \\ \vdots & & \ddots & & \vdots \\ 0 & 0 & \cdots & \cdots & m_N \end{bmatrix}, \tag{B.10}$$

$$\hat{\mathbf{K}}_{\text{elas}} = \begin{bmatrix} \mathbf{K}_{\text{elas}}^{(0)} & & \\ & \ddots & \\ & & \mathbf{K}_{\text{elas}}^{(2J+1)} \end{bmatrix} \quad , \quad \mathbf{K}_{\text{elas}}^{(a)} = k_{\text{r}}\alpha \begin{bmatrix} 2 & -1 & 0 & \cdots & 0 \\ -1 & 2 & -1 & & 0 \\ 0 & \ddots & \ddots & \ddots & \vdots \\ \vdots & & \ddots & & -1 \\ 0 & 0 & \cdots & -1 & 1 \end{bmatrix},$$

$$\hat{\mathbf{K}}_{\text{hyst}} = \begin{bmatrix} \mathbf{K}_{\text{hyst}}^{(0)} & & \\ & \ddots & \\ & & \mathbf{K}_{\text{hyst}}^{(2J+1)} \end{bmatrix} \quad , \quad \mathbf{K}_{\text{hyst}}^{(a)} = k_{\text{r}}\left(1-\alpha\right) \begin{bmatrix} 2 & -1 & 0 & \cdots & 0 \\ -1 & 2 & -1 & & 0 \\ 0 & \ddots & \ddots & \ddots & \vdots \\ \vdots & & \ddots & & -1 \\ 0 & 0 & \cdots & -1 & 1 \end{bmatrix},$$

$$\hat{\mathbf{F}}_{\text{nl}} = \begin{bmatrix} \mathbf{F}_{\text{nl}}{}^{(0)} & \mathbf{F}_{\text{nl}}{}^{(1)} & \cdots & \mathbf{F}_{\text{nl}}{}^{(2J+1)} \end{bmatrix}^{\text{T}} \quad , \quad \mathbf{F}_{\text{nl}}{}^{(a)} = \begin{bmatrix} f_{\text{nl}}^{(1)} & f_{\text{nl}}^{(2)} & \cdots f_{\text{nl}}^{(N)} \end{bmatrix}^{\text{T}},$$

$$\hat{\mathbf{F}}_{\text{ext}} = \begin{bmatrix} \mathbf{F}_{\text{ext}}{}^{(0)} & \mathbf{F}_{\text{ext}}{}^{(1)} & \cdots & \mathbf{F}_{\text{ext}}{}^{(2J+1)} \end{bmatrix}^{\text{T}} \quad , \quad \mathbf{F}_{\text{ext}}{}^{(a)} = \begin{bmatrix} f_{\text{ext}}^{(1)} & f_{\text{ext}}^{(2)} & \cdots f_{\text{ext}}^{(N)} \end{bmatrix}^{\text{T}},$$

$$a = 1 \ldots 2J+1 \tag{B.11}$$

The derivatives of each harmonic are computed by the derivative matrix $\hat{\mathbf{D}}$, which is given by

$$\hat{\mathbf{D}} = \begin{bmatrix} \mathbf{0} & \mathbf{0} & \cdots & \mathbf{0} \\ \mathbf{0} & \mathbf{D}^{(1)} & \cdots & \mathbf{0} \\ \vdots & \vdots & \ddots & \vdots \\ \mathbf{0} & \mathbf{0} & \cdots & \mathbf{D}^{(J)} \end{bmatrix} \quad , \quad \mathbf{D}^{(j)} = \begin{bmatrix} 0 & 0 & \cdots & 0 & j\Omega & 0 & \cdots & 0 \\ 0 & 0 & \cdots & 0 & 0 & j\Omega & \cdots & 0 \\ \vdots & \vdots & \ddots & \vdots & \vdots & \vdots & \ddots & \vdots \\ 0 & 0 & \cdots & 0 & 0 & 0 & \cdots & j\Omega \\ -j\Omega & 0 & \cdots & 0 & 0 & 0 & \cdots & 0 \\ 0 & -j\Omega & \cdots & 0 & 0 & 0 & \cdots & 0 \\ \vdots & \vdots & \ddots & \vdots & \vdots & \vdots & \cdots & \vdots \\ 0 & 0 & \cdots & -j\Omega & 0 & 0 & \cdots & 0 \end{bmatrix}. \tag{B.12}$$

Then, from Eq. (B.9), $\tilde{\mathbf{z}}$ can be expressed in terms of $\tilde{\mathbf{u}}$ according to

$$\tilde{\mathbf{z}} = \left(\hat{\mathbf{K}}_{\text{hyst}}\right)^{-1} \left(\hat{\mathbf{F}}_{\mathbf{ext}} - \hat{\mathbf{M}}\hat{\mathbf{D}}\hat{\mathbf{D}}\tilde{\mathbf{u}} - \hat{\mathbf{K}}_{\text{rest}}\tilde{\mathbf{u}}\right). \tag{B.13}$$

The formulation now contains only a single unknown vector $\tilde{\mathbf{u}}$. Next, by using the IDFT, as presented in Eq. (20), the response is transformed from the frequency to the time domain. To solve $\tilde{\mathbf{u}}$, residual functions are used to solve the system in an iterative manner. The residuals are chosen based on the satisfaction of Eq. (B.1), so for an NDOF system the residual functions become

$$\begin{aligned} r^{(1)} &= \dot{z}^{(1)} - \dot{u}^{(1)} \left\{\kappa - \left[\gamma_{\text{b}} + \beta_{\text{b}} \operatorname{sgn}\left(\dot{u}^{(1)}\right) \operatorname{sgn}\left(z^{(1)}\right)\right] |z^{(1)}|^n\right\}, \\ &\vdots, \\ r^{(N)} &= \dot{z}^{(N)} - \dot{u}^{(N)} \left\{\kappa - \left[\gamma_{\text{b}} + \beta_{\text{b}} \operatorname{sgn}\left(\dot{u}^{(N)}\right) \operatorname{sgn}\left(z^{(N)}\right)\right] |z^{(N)}|^n\right\}, \end{aligned} \tag{B.14}$$

shortly denoted as $\mathbf{r}$, written as

$$\mathbf{r} = \left[r^{(1)} \cdots r^{(N)}\right]^{\text{T}}. \tag{B.15}$$

For solving the system, an iterative procedure is required as stated in Eq. (22), with $\tilde{\mathbf{J}}$ defined as

$$\tilde{\mathbf{J}} = \frac{\partial \tilde{\mathbf{r}}}{\partial \tilde{\mathbf{u}}}, \tag{B.16}$$

which implies that for each residual function the partial derivatives with respect to the state vector needs to be determined. The partial derivatives

of the residual in the time domain $\mathbf{r}$ with respect to the state vectors $\tilde{\mathbf{u}}$ are given by the Jacobian in the time domain $\mathbf{J}$,

$$\mathbf{J} = \frac{\partial \mathbf{r}\left(\dot{\mathbf{u}}, \mathbf{z}, \dot{\mathbf{z}}\right)}{\partial \tilde{\mathbf{u}}} = \frac{\partial \mathbf{r}}{\partial \dot{\mathbf{u}}}\frac{\partial \dot{\mathbf{u}}}{\partial \tilde{\mathbf{u}}} + \frac{\partial \mathbf{r}}{\partial \mathbf{z}}\frac{\partial \mathbf{z}}{\partial \tilde{\mathbf{u}}} + \frac{\partial \mathbf{r}}{\partial \dot{\mathbf{z}}}\frac{\partial \dot{\mathbf{z}}}{\partial \tilde{\mathbf{u}}}. \tag{B.17}$$

For the sake of brevity, the partial derivatives can be found in Appendix C. Once the partial derivatives are derived, $\mathbf{J}$ is computed according to Eq. (B.17) and transformed back to the frequency domain by using the DFT, see Eq. (26). Together they form $\tilde{\mathbf{J}}$, according to the partitioned form

$$\tilde{\mathbf{J}} = \left[\frac{\partial \mathbf{a}_0}{\tilde{\mathbf{u}}} \quad \frac{\partial \mathbf{a}_j}{\tilde{\mathbf{u}}} \quad \frac{\partial \mathbf{b}_j}{\tilde{\mathbf{u}}}\right]^{\mathrm{T}}. \tag{B.18}$$

Finally, the residual vector $\mathbf{r}$ is also converted to the frequency domain by using the DFT, hence

$$\begin{aligned}
\tilde{\mathbf{r}}_{\mathrm{a}}^{(0)} &= \frac{1}{M}\sum_{p=0}^{M-1}\mathbf{r}_p, \\
\tilde{\mathbf{r}}_{\mathrm{a}}^{(j)} &= \frac{2}{M}\sum_{p=0}^{M-1}\left[\mathbf{r}_p \cos\left(\frac{2\pi p j}{M}\right)\right], \\
\tilde{\mathbf{r}}_{\mathrm{b}}^{(j)} &= \frac{2}{M}\sum_{p=0}^{M-1}\left[\mathbf{r}_p \sin\left(\frac{2\pi p j}{M}\right)\right].
\end{aligned} \tag{B.19}$$

This process is repeated until convergence is reached according to Eq. (23) and summarized in Figure B.12.

Appendix B.3. Case study

To show the performance of the AFTHBM, applied on an NDOF Bouc-Wen model, a case study is performed on a concrete shear beam with a unit square area, subjected by a harmonic force at the first DOF as presented in Figure B.13. For validation purposes, the influence of the nonlinearity in the model is put to almost zero (not exactly to prevention singularities of $\tilde{\mathbf{J}}$) and the motion at the tip of the beam ($z = 0$) is compared with the equivalent linear system, see Figure B.14. The total material behaviour is governed by the elastic and hysteretic stiffness, so no additional stiffness or viscous damping is present. The system is subjected to a forcing frequency which

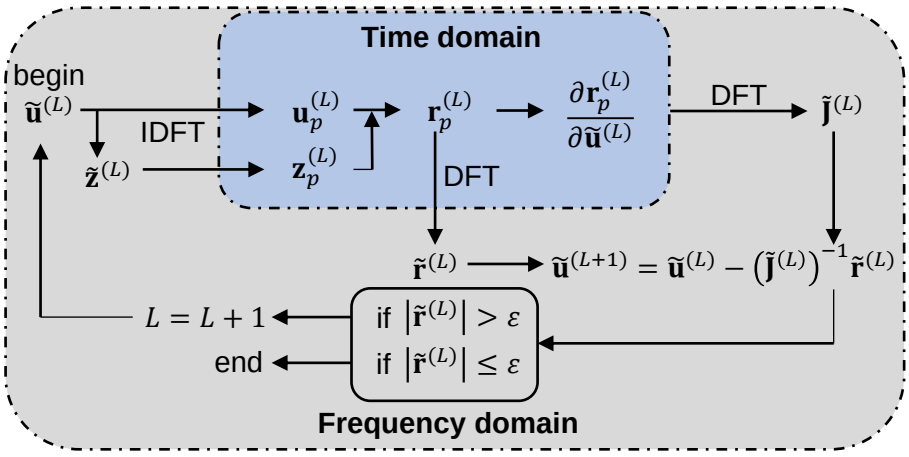

Figure B.12: Principle of the AFTHBM, applied on shear beam. The procedure starts with assuming an initial ($L = 0$) state vector $\tilde{\mathbf{u}}$, see upper left and ends when the tolerances are satisfied (bottom center). The scheme is borrowed and extended from the work of van Til [34] and Wong [17, 39] et al.

is close to the first resonance frequency. The behaviour of the hysteretic properties of the system become more dominant in this highly nonlinear regime. This results in the appearance of higher order harmonics. The results for the nonlinear case are presented in Figure B.15. The influence of higher order harmonics can be made more clear by using a spectrum, see figure B.16. As can be observed in Figure B.16, due to limited sampling or non-strict tolerances, the harmonic of order $J = 0$, is not exactly zero. The higher the order of the considered harmonic, the lower the amplitude. All the even harmonics are almost zero. The system with the Bouc-wen model can easier reach convergence due to the smooth transition from the loading to the unloading branches. This indicates that computations can be faster performed because less time samples are required in comparision with Masing hysteresis. However, not to lose much accuracy, M cannot be too low. This is especially the case when the system reacts very stiff. A higher sampling rate is then required to guarantee convergence and prevent ill-conditioning of the Jacobian. The system exhibits softening behaviour which is depicted in Figure B.17. This can be observed by the shift of the peaks in the FRCs to the left. To reduce the computation time, the input for the next forcing frequency is based on the previous result. Consequently, less iterations are needed in order to obtain convergence.

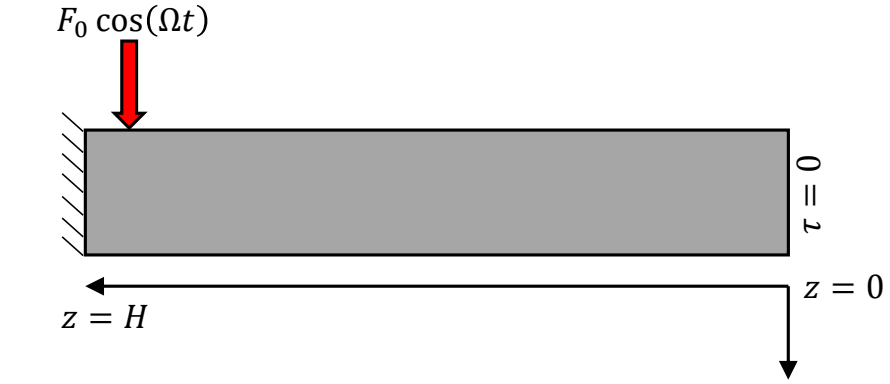

(a) Continuous description of the model.

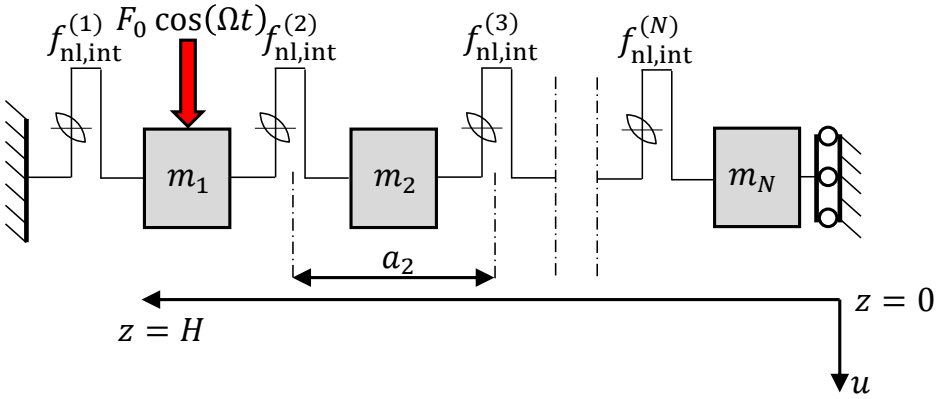

(b) Lattice description of the model.

Figure B.13: Model description of a concrete shear beam with hysteretic damping and unit square area subjected to harmonic excitation at the first DOF. The beam is clamped at $z = H$ an has a free boundary condition at $z = 0$. (a) Represents the continuous description, (b) the discretised system (lattice model). Used parameters are: $H = 20$m, $\rho = 2,500$ kg $\cdot$ m^{-3}, $G_0 = 11,500 \cdot 10^6$ N $\cdot$ m^{-2}, $F_0 = 900,000$ N, $N = 10$. The figure has been rotated 90 degrees clockwise.

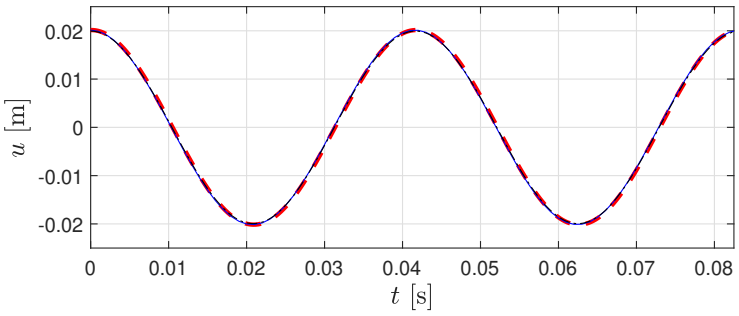

Figure B.14: Motion at the tip of the beam $z = 0$ m for the linear case. ▪▪▪Motion computed by AFTHBM. - - -Motion of the linear system. —Time-integration results by ODE45 in MATLAB. Used parameters of the model (in addition to figure B.13): $\kappa = 1$, $\gamma_{\mathrm{b}} = -1$, $\beta_{\mathrm{b}} = 2$, $n = 2$, $\alpha = 0.99$, $M = 2^7$, $\Omega = 150.8$ rad/s, $J = 1$, $\epsilon = 10^{-10}$.

Appendix C. Derivation of the analytical derivatives of the Bouc-Wen model

$$\frac{\partial \mathbf{r}}{\partial \dot{\mathbf{u}}} = \begin{bmatrix} \frac{\partial r^{(1)}}{\partial \dot{u}^{(1)}} & \frac{\partial r^{(1)}}{\partial \dot{u}^{(2)}} & \cdots & \frac{\partial r^{(1)}}{\partial \dot{u}^{(N)}} \\ \frac{\partial r^{(2)}}{\partial \dot{u}^{(1)}} & \frac{\partial r^{(2)}}{\partial \dot{u}^{(2)}} & \cdots & \frac{\partial r^{(2)}}{\partial \dot{u}^{(N)}} \\ \vdots & \vdots & \ddots & \vdots \\ \frac{\partial r^{(N)}}{\partial \dot{u}^{(1)}} & \frac{\partial r^{(N)}}{\partial \dot{u}^{(2)}} & \cdots & \frac{\partial r^{(N)}}{\partial \dot{u}^{(N)}} \end{bmatrix} \tag{C.1}$$

Where from Eq. (C.1)

$$\frac{\partial r^{(d)}}{\partial \dot{u}^{(a)}} = \delta_{d,a} \left\{ \left[\gamma_{\mathrm{b}} + \beta_{\mathrm{b}} \operatorname{sgn}\left(\dot{u}_a\right) \operatorname{sgn}\left(z_d\right) \right] |z_d|^n + \dot{u}_a \beta_{\mathrm{b}} 2\delta\left(\dot{u}_a\right) \operatorname{sgn}\left(z_d\right) |z_d|^n - \kappa \right\} \tag{C.2}$$

and $\delta_{d,a}$ denotes the Kronecker delta, defined as

$$\begin{cases} 1 & \text{if} \quad d = a, \\ 0 & \text{otherwise}, \end{cases} \tag{C.3}$$

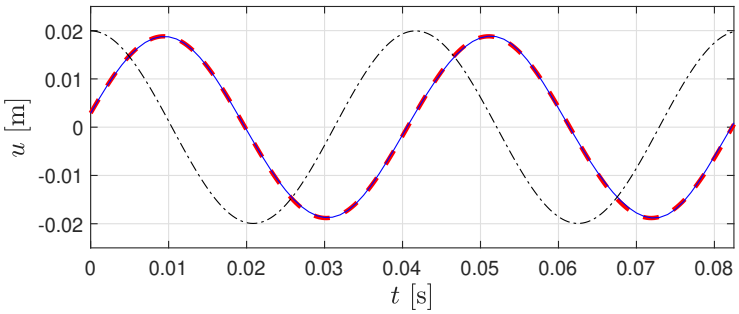

(a) Response with $J = 1$.

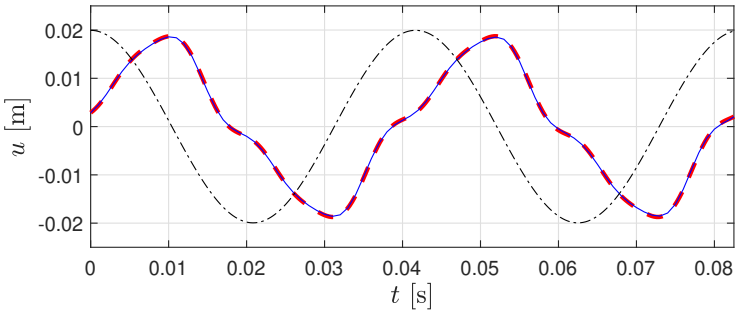

(b) Response with $J = 5$.

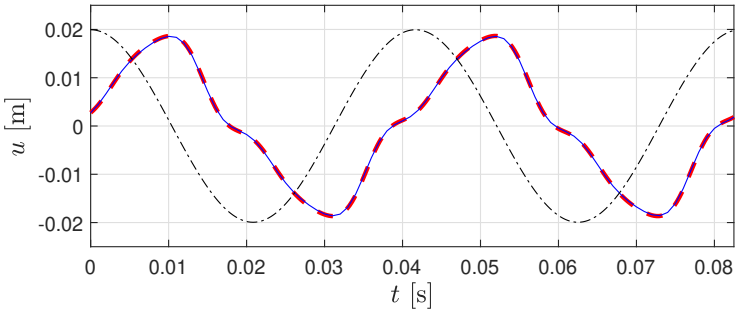

(c) Response with $J = 9$.

Figure B.15: Motion at the tip of the beam $z = 0$ m for the nonlinear case for different amounts of harmonics. (a) $J = 1$, (b) $J = 5$, (c) $J = 9$. ▪▪▪Motion computed by AFTHBM. - - -Motion of the linear system. ——Time-integration results by ODE45 in MATLAB. Used parameters of the model (in addition to Figure B.13): $\kappa = 1$, $\gamma_{\mathrm{b}} = 150$, $\beta_{\mathrm{b}} = 151$, $n = 2$, $\alpha = 0.1$, $M = 2^7$, $\Omega = 150.8$ rad/s, $\epsilon = 10^{-10}$.

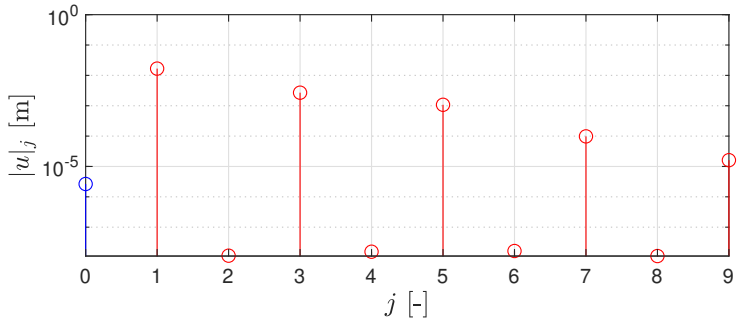

Figure B.16: Spectrum for DOF $i = N$ at the tip of the beam $z = 0$ m for the nonlinear case. ○ 0-th harmonic, nonzero due to limited sampling and nonstrict tolerances. ○ Harmonics $1 - 9$. Note that higher order harmonics have a lower magnitude. For the analysis the same parameters have been used as presented in Figure B.15.

and δ the Dirac-Delta function.

$$\frac{\partial \dot{\mathbf{u}}}{\partial \tilde{\mathbf{u}}} = \begin{bmatrix} \frac{\partial \dot{u}^{(1)}}{\partial a_0^{(1)}} & \cdots & \frac{\partial \dot{u}^{(1)}}{\partial a_0^{(N)}} & \frac{\partial \dot{u}^{(1)}}{\partial a_j^{(1)}} & \cdots & \frac{\partial \dot{u}^{(1)}}{\partial a_j^{(N)}} & \frac{\partial \dot{u}^{(1)}}{\partial b_j^{(1)}} & \cdots & \frac{\partial \dot{u}^{(1)}}{\partial b_j^{(N)}} \\ \frac{\partial \dot{u}^{(2)}}{\partial a_0^{(1)}} & \cdots & \frac{\partial \dot{u}^{(2)}}{\partial a_0^{(N)}} & \frac{\partial \dot{u}^{(2)}}{\partial a_j^{(1)}} & \cdots & \frac{\partial \dot{u}^{(2)}}{\partial a_j^{(N)}} & \frac{\partial \dot{u}^{(2)}}{\partial b_j^{(1)}} & \cdots & \frac{\partial \dot{u}^{(2)}}{\partial b_j^{(N)}} \\ \vdots & \ddots & \vdots & \vdots & \ddots & \vdots & \vdots & \ddots & \vdots \\ \frac{\partial \dot{u}^{(N)}}{\partial a_0^{(1)}} & \cdots & \frac{\partial \dot{u}^{(N)}}{\partial a_0^{(N)}} & \frac{\partial \dot{u}^{(N)}}{\partial a_j^{(1)}} & \cdots & \frac{\partial \dot{u}^{(N)}}{\partial a_j^{(N)}} & \frac{\partial \dot{u}^{(N)}}{\partial b_j^{(1)}} & \cdots & \frac{\partial \dot{u}^{(N)}}{\partial b_j^{(N)}} \end{bmatrix} \tag{C.4}$$

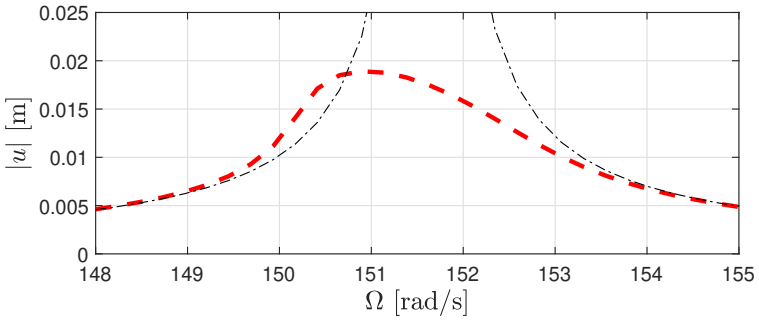

(a) FRC with $J = 1$.

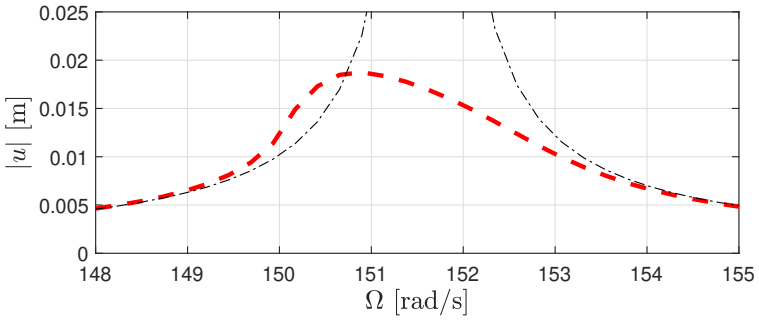

(b) FRC with $J = 5$.

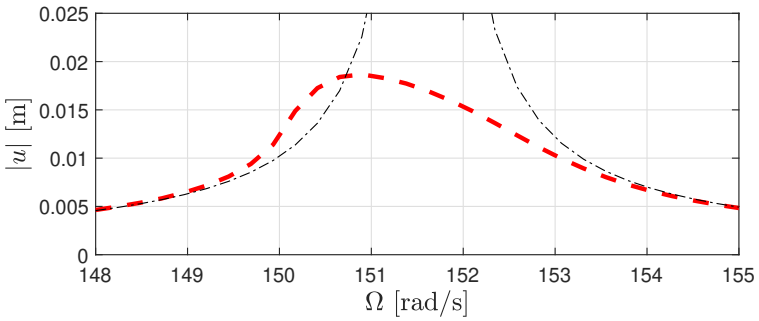

(c) FRC with $J = 9$.

Figure B.17: FRCs at the tip of the beam $z = 0$ m for the nonlinear case for different amounts of harmonics. (a) $J = 1$, (b) $J = 5$, (c) $J = 9$. ▪▪▪Motion computed by AFTHBM. - · - Motion of the linear system. Used parameters of the model (in addition to figure B.13): $\kappa = 1$, $\gamma_\mathrm{b} = 150$, $\beta_\mathrm{b} = 151$, $n = 2$, $\alpha = 0.1$, $M = 2^7$, $\Omega = 148 - 153$ rad/s, $N\Omega = 30$, $\epsilon = 10^{-10}$.

Where from Eq. (C.4)

$$\frac{\partial \dot{u}^{(a)}}{\partial a_0^{(e)}} = 0 \quad \text{for} \quad a = 1, ..., N, \ e = 0, ..., N, \tag{C.5}$$

$$\frac{\partial \dot{u}^{(a)}}{\partial a_j^{(e)}} = -j\delta_{a,e}\Omega \sin(\Omega t) \quad \text{for} \quad j = 1, ..., J,$$

$$\frac{\partial \dot{u}^{(a)}}{\partial b_j^{(e)}} = j\delta_{a,e}\Omega \cos(\Omega t) \quad \text{for} \quad j = 1, ..., J.$$

$$\frac{\partial \mathbf{r}}{\partial \mathbf{z}} = \begin{bmatrix} \frac{\partial r^{(1)}}{\partial z^{(1)}} & \frac{\partial r^{(1)}}{\partial z^{(2)}} & \cdots & \frac{\partial r^{(1)}}{\partial z^{(N)}} \\ \frac{\partial r^{(2)}}{\partial z^{(1)}} & \frac{\partial r^{(2)}}{\partial z^{(2)}} & \cdots & \frac{\partial r^{(2)}}{\partial z^{(N)}} \\ \vdots & \vdots & \ddots & \vdots \\ \frac{\partial r^{(N)}}{\partial z^{(1)}} & \frac{\partial r^{(N)}}{\partial z^{(2)}} & \cdots & \frac{\partial r^{(N)}}{\partial z^{(N)}} \end{bmatrix} \tag{C.6}$$

Where from Eq. (C.6)

$$\frac{\partial r^{(d)}}{\partial z^{(a)}} = \delta_{d,a}\{\dot{u}_a \beta_{\mathrm{b}} \operatorname{sgn}(\dot{u}_a) 2\delta(z_d) |z_d|^n + \dot{u}_a [\gamma_{\mathrm{b}} + \beta_{\mathrm{b}} \operatorname{sgn}(\dot{u}_a) \operatorname{sgn}(z_d) |z_d|^n n \operatorname{sgn}(z_d)] / |z_d|\} \tag{C.7}$$

$$\frac{\partial \mathbf{z}}{\partial \tilde{\mathbf{u}}} = \begin{bmatrix} \frac{\partial z^{(1)}}{\partial a_0^{(1)}} & \cdots & \frac{\partial z^{(1)}}{\partial a_0^{(N)}} & \frac{\partial z^{(1)}}{\partial a_j^{(1)}} & \cdots & \frac{\partial z^{(1)}}{\partial a_j^{(N)}} & \frac{\partial z^{(1)}}{\partial b_j^{(1)}} & \cdots & \frac{\partial z^{(1)}}{\partial b_j^{(N)}} \\ \frac{\partial z^{(2)}}{\partial a_0^{(1)}} & \cdots & \frac{\partial z^{(2)}}{\partial a_0^{(N)}} & \frac{\partial z^{(2)}}{\partial a_j^{(1)}} & \cdots & \frac{\partial z^{(2)}}{\partial a_j^{(N)}} & \frac{\partial z^{(2)}}{\partial b_j^{(1)}} & \cdots & \frac{\partial z^{(2)}}{\partial b_j^{(N)}} \\ \vdots & \ddots & \vdots & \vdots & \ddots & \vdots & \vdots & \ddots & \vdots \\ \frac{\partial z^{(N)}}{\partial a_0^{(1)}} & \cdots & \frac{\partial z^{(N)}}{\partial a_0^{(N)}} & \frac{\partial z^{(N)}}{\partial a_j^{(1)}} & \cdots & \frac{\partial z^{(N)}}{\partial a_j^{(N)}} & \frac{\partial z^{(N)}}{\partial b_j^{(1)}} & \cdots & \frac{\partial z^{N}}{\partial b_j^{(N)}} \end{bmatrix} \tag{C.8}$$

Where from Eq. (C.8)

$$\frac{\partial z^{(a)}}{\partial a_0^{(e)}} = \begin{cases} \dfrac{\alpha k_{\mathrm{r}}}{(-1+\alpha)\, k_{\mathrm{r}}} & \text{if} \quad a = e, \\ 0 & \text{otherwise}, \end{cases} \tag{C.9}$$

$$\frac{\partial z^{(a)}}{\partial a_j^{(e)}} = \begin{cases} \dfrac{(-e m_e \Omega^2 j^2 + \alpha k_{\mathrm{r}}) \cos(\Omega t)}{(-1+\alpha)\, k_{\mathrm{r}}} & \text{if} \quad a = e, \\ -\dfrac{e \Omega^2 j^2 m_e \cos(\Omega t)}{(-1+\alpha)\, k_{\mathrm{r}}} & \text{otherwise}, \end{cases}$$

$$\frac{\partial z^{(a)}}{\partial b_j^{(e)}} = \begin{cases} \dfrac{(-e m_e \Omega^2 j^2 + \alpha k_{\mathrm{r}}) \sin(\Omega t)}{(-1+\alpha)\, k_{\mathrm{r}}} & \text{if} \quad a = e, \\ -\dfrac{e \Omega^2 j^2 m_e \sin(\Omega t)}{(-1+\alpha)\, k_{\mathrm{r}}} & \text{otherwise}. \end{cases} \tag{C.10}$$

$$\frac{\partial \mathbf{r}}{\partial \dot{\mathbf{z}}} = \begin{bmatrix} \frac{\partial r^{(1)}}{\partial \dot{z}^{(1)}} & \frac{\partial r^{(1)}}{\partial \dot{z}^{(2)}} & \cdots & \frac{\partial r^{(1)}}{\partial \dot{z}^{(N)}} \\ \frac{\partial r^{(2)}}{\partial \dot{z}^{(1)}} & \frac{\partial r^{(2)}}{\partial \dot{z}^{(2)}} & \cdots & \frac{\partial r^{(2)}}{\partial \dot{z}^{(N)}} \\ \vdots & \vdots & \ddots & \vdots \\ \frac{\partial r^{(N)}}{\partial \dot{z}^{(1)}} & \frac{\partial r^{(N)}}{\partial \dot{z}^{(2)}} & \cdots & \frac{\partial r^{(N)}}{\partial \dot{z}^{(N)}} \end{bmatrix} \tag{C.11}$$

$$\frac{\partial \dot{\mathbf{z}}}{\partial \tilde{\mathbf{u}}} = \begin{bmatrix} \frac{\partial \dot{z}^{(1)}}{\partial a_0^{(1)}} & \cdots & \frac{\partial \dot{z}^{(1)}}{\partial a_0^{(N)}} & \frac{\partial \dot{z}^{(1)}}{\partial a_j^{(1)}} & \cdots & \frac{\partial \dot{z}^{(1)}}{\partial a_j^{(N)}} & \frac{\partial \dot{z}^{(1)}}{\partial b_j^{(1)}} & \cdots & \frac{\partial \dot{z}^{(1)}}{\partial b_j^{(N)}} \\ \frac{\partial \dot{z}^{(2)}}{\partial a_0^{(1)}} & \cdots & \frac{\partial \dot{z}^{(2)}}{\partial a_0^{(N)}} & \frac{\partial \dot{z}^{(2)}}{\partial a_j^{(1)}} & \cdots & \frac{\partial \dot{z}^{(2)}}{\partial a_j^{(N)}} & \frac{\partial \dot{z}^{(2)}}{\partial b_j^{(1)}} & \cdots & \frac{\partial \dot{z}^{(2)}}{\partial b_j^{(N)}} \\ \vdots & \ddots & \vdots & \vdots & \ddots & \vdots & \vdots & \ddots & \vdots \\ \frac{\partial \dot{z}^{(N)}}{\partial a_0^{(1)}} & \cdots & \frac{\partial \dot{z}^{(N)}}{\partial a_0^{(N)}} & \frac{\partial \dot{z}^{(N)}}{\partial a_j^{(1)}} & \cdots & \frac{\partial \dot{z}^{N}}{\partial a_j^{(N)}} & \frac{\partial \dot{z}^{(N)}}{\partial b_j^{(1)}} & \cdots & \frac{\partial \dot{z}^{(N)}}{\partial b_j^{(N)}} \end{bmatrix} \tag{C.12}$$

Where from Eq. (C.12)

$$\frac{\partial \dot{z}^{(a)}}{\partial a_0^{(e)}} = 0, \tag{C.13}$$

$$\frac{\partial \dot{z}^{(a)}}{\partial a_j^{(e)}} = \begin{cases} -\dfrac{\left[\left(-e\Omega^2 j^2 m_e + \alpha k_{\mathrm{r}}\right)\sin\left(\Omega t\right)\right] j\Omega}{\left(-1+\alpha\right) k_{\mathrm{r}}} & \text{if} \quad a = e, \\ \dfrac{e\Omega^3 j^3 m_e \sin\left(\Omega t\right)}{\left(-1+\alpha\right) k_{\mathrm{r}}} & \text{otherwise,} \end{cases}$$

$$\frac{\partial \dot{z}^{(a)}}{\partial b_j^{(e)}} = \begin{cases} -\dfrac{\left[\left(e\Omega^2 j^2 m_e - \alpha k_{\mathrm{r}}\right)\cos\left(\Omega t\right)\right] j\Omega}{\left(-1+\alpha\right) k_{\mathrm{r}}} & \text{if} \quad a = e, \\ -\dfrac{-e\Omega^3 j^3 m_e \cos\left(\Omega t\right)}{\left(-1+\alpha\right) k_{\mathrm{r}}} & \text{otherwise.} \end{cases}$$

References

[1] G. E. Engineering, Geotechnical Earthquake Engineering, 1996.

[2] M. Arefi, M. Cubrinovski, B. Bradley, A model for nonlinear total stress analysis with consistent stiffness and damping variation (2012).

[3] D.-Y. Chiang, The generalized masing models for deteriorating hysteresis and cyclic plasticity, Applied Mathematical Modelling 23 (1999) 847–863.

[4] Darendelli, Development of a new family of normalized modulus reduction and material damping curves, 2001.

[5] B. O. Hardin, V. P. Drnevich, Shear modulus and damping in soils: Design equations and curves, Geotechnical Special Publication (2002) 1459–1484.

[6] S.-H. Chong, Soil dynamic constitutive model for characterizing the nonlinear-hysteretic response, Applied Sciences 7 (2017) 1110.

[7] M. Krack, J. Gross, Harmonic Balance for Nonlinear Vibration Problems, 2019.

[8] J. Jia, Dynamic and cyclic properties of soils, in: Soil Dynamics and Foundation Modeling, Springer, 2018, pp. 75–108.

[9] Z. Wu, D. Zhang, T. Zhao, J. Ma, D. Zhao, An experimental research on damping ratio and dynamic shear modulus ratio of frozen silty clay of the qinghai-tibet engineering corridor, Transportation Geotechnics 21 (2019) 100269.

[10] B. D'Elia, G. Lanzo, A. Pagliaroli, Small-strain stiffness and damping of soils in a direct simple shear device, in: Pacific conference on earthquake engineering, pp. 1–8.

[11] J. Pruiksma, Nonlinear and equivalent linear site response analysis for the groningen area, 2016.

[12] J. J. Thomsen, Vibrations and Stability, McGraw-Hill, 1997.

[13] J. H. Wang, W. K. Chen, Investigation of the vibration of a blade with friction damper by HBM, Journal of Engineering for Gas Turbines and Power 115 (1993) 294–299.

[14] Y. Li, Y. Dong, Y. Qin, H. Lv, Nonlinear forced vibration and stability of an axially moving viscoelastic sandwich beam, International Journal of Mechanical Sciences 138 (2018) 131–145.

[15] A. H. Nayfeh, B. Balachandran, Applied nonlinear dynamics: analytical, computational, and experimental methods, John Wiley & Sons, 2008.

[16] R. Seydel, Practical Bifurcation and Stability Analysis, volume 5, Springer, Koln, third edit edition, 2009.

[17] Steady-State Oscillation of Hysteretic Differential Model - Part I: Response Analysis 120 (1995) 2299–2325.

[18] G. Papazafeiropoulos, Arc-length method, 2014.

[19] M. Ritto-Corrêa, D. Camotim, On the arc-length and other quadratic control methods: Established, less known and new implementation procedures, Computers and Structures COMPUT STRUCT 86 (2008) 1353–1368.

[20] P. Bergan, G. Horrigmoe, B. Krakeland, T. Soreide, Solution techniques for non-linear finite element problems, 1978.

[21] L. Yuanqi, S. Zuyan, Improvements on the arc-length-type method, Acta Mechanica Sinica - ACTA MECH SINICA 20 (2004) 541–550.

[22] D. Capecchi, R. Masiani, F. Vestroni, Periodic and non-periodic oscillations of a class of hysteretic two degree of freedom systems, Nonlinear Dynamics 13 (1997) 309–325.

[23] W. D. Iwan, The steady-state response of the double bilinear hysteretic model (1965).

[24] D. Capecchi, R. Masiani, Reduced phase space analysis for hysteretic oscillators of masing type, Chaos, Solitons & Fractals 7 (1996) 1583–1600.

[25] W. Lacarbonara, F. Vestroni, Nonclassical Responses of Oscillators with Hysteresis, Nonlinear dynamics 32 (2003) 235–258.

[26] P. Casini, F. Vestroni, Nonlinear resonances of hysteretic oscillators, Acta Mechanica 229 (2018) 939–952.

[27] J. Zhang, E. Sulollari, F. Faragau, Andrei B. Pisano, P. van der Male, M. Martinelli, A. Metrikine, K. van Dalen, Harmonic balance method for the stationary response of finite and semi-infinite nonlinear dissipative continua: three canonical problems, 2020.

[28] J. Shi, D. Asimaki, From stiffness to strength: Formulation and validation of a hybrid hyperbolic nonlinear soil model for site-response analyses, Bulletin of the Seismological Society of America 107 (2017) 1336–1355.

[29] S. Yniesta, S. Brandenberg, Unloading-reloading rule for nonlinear site response analysis (2015).

[30] T. Cameron, J. H. Griffin, An alternating frequency/time domain method for calculating the steady-state response of nonlinear dynamic systems (1989).

[31] E. Chatelet, D. Rade, G. Jacquet-Richardet, Dynamic behaviour of cyclic symmetrical n dof system in the presence of dry friction, HAL, 2013.

[32] T.-C. Yuan, J. Yang, L.-Q. Chen, A harmonic balance approach with alternating frequency/time domain progress for piezoelectric mechanical systems, Mechanical Systems and Signal Processing 120 (2019) 274–289.

[33] C. Joannin, B. Chouvion, F. Thouverez, J.-P. Ousty, M. Mbaye, A nonlinear component mode synthesis method for the computation of steady-state vibrations in non-conservative systems, Mechanical Systems and Signal Processing 83 (2017) 75–92.

[34] J. van Til, F. Alijani, S. N. Voormeeren, W. Lacarbonara, Frequency domain modeling of nonlinear end stop behavior in Tuned Mass Damper systems under single- and multi-harmonic excitations, Journal of Sound and Vibration 438 (2019) 139–152.

[35] N. A. F. Senan, A brief introduction to using ode45 in matlab, University of California at Berkeley, USA (2007).

[36] D. Kaltsas, Modelling of the dynamic pressuremeter test in porous soil using analytical and numerical methods, 2016.

[37] R. K., C. R., M. R., B. B., Drilled Shaft Side Friction in Gravelly Soils, Journal of Geotechnical and Geoenvironmental Engineering 131 (2005) 987–1003.

[38] J. Zhang, R. D. Andrus, C. H. Juang, Normalized shear modulus and material damping ratio relationships, Journal of Geotechnical and Geoenvironmental Engineering 131 (2005) 453–464.

[39] Steady-State Oscillation of Hysteretic Differential Model - Part II: Performance Analysis 120 (1995) 2271–2298.

[40] C. Phillips, Y. M. Hashash, Damping formulation for nonlinear 1d site response analyses, Soil Dynamics and Earthquake Engineering 29 (2009) 1143–1158.

[41] M. Krack, L. Panning-von Scheidt, J. Wallaschek, A high-order harmonic balance method for systems with distinct states, Journal of Sound and Vibration 332 (2013) 5476–5488.

[42] C. Mack, Fundamental principles of optical lithography: the science of microfabrication, John Wiley & Sons, 2008.

[43] P. Vigué, C. Vergez, S. Karkar, B. Cochelin, Regularized friction and continuation: Comparison with coulomb's law, Journal of Sound and Vibration 389 (2017) 350–363.

[44] A. Brandt, Noise and Vibration Analysis, Wiley, 2011.

[45] C. Glocker, Set-valued force laws: dynamics of non-smooth systems, volume 1, Springer Science & Business Media, 2013.

[46] J. Guillen, C. Pierre, An efficient, hybrid, frequency-time domain method for the dynamics of large-scale dry-friction damped structural systems., in: IUTAM symposium on unilateral multibody contacts, Springer, pp. 169–178.

[47] M. Ismail, F. Ikhouane, J. Rodellar, The hysteresis bouc-wen model, a survey, Archives of Computational Methods in Engineering 16 (2009) 161–188.

[48] X. Zhu, X. Lu, Parametric identification of bouc-wen model and its application in mild steel damper modeling, Procedia Engineering 14 (2011) 318–324.

[49] W. Beuckelaers, Fatigue Life Calculation of Monopiles for Offshore Wind Turbines using a Kinematic Hardening Soil Model, Proceedings of the 24th European Young Geotechnical Engineering Conference (EYGEC) (2015) 26–29.